INTERNATIONAL JOURNAL FOR NUMERICAL METHODS IN FLUIDS
Int. J. Numer. Meth. Fluids 2000; **33**: 499–534

On simulation of outflow boundary conditions in finite difference calculations for incompressible fluid

M. A. Ol'shanskii* and V. M. Staroverov

Department of Mechanics and Mathematics, Moscow State University, Moscow, Russian Federation

SUMMARY

For incompressible Navier–Stokes equations in primitive variables, a method of setting absorbing outflow boundary conditions on an artificial boundary is considered. The advection equations used on the outflow boundary are convenient for finite difference (FD) methods, where a weak formulation of a problem is inapplicable. An unsteady viscous incompressible Navier–Stokes flow in a channel with a moving damper is modeled. An accurate comparison and analysis of numerical and mechanical situations are carried out for a variety of boundary conditions and Reynolds numbers. The proposed outflow conditions provide that the problem with Dirichlet boundary conditions should be solved on each time step. Copyright © 2000 John Wiley & Sons, Ltd.

KEY WORDS: artificial boundary; finite differences; incompressible flows; outflow conditions

1. INTRODUCTION

In this paper we present and discuss an approach to the numerical simulation of outflow boundary conditions for an unsteady incompressible Navier–Stokes flow. A first-order advection equation is used on an artificial boundary. The advection velocity is the velocity of a typical flow, and it is allowed to vary along the boundary. For a small perturbation of a linear flow when the linearized analysis is valid, the proposed conditions are justified by the techniques of Halpern and Schatzman [1] and a scaling method of Hagstrom [2]. For a close artificial boundary and essential non-linear flow, these conditions seem reasonable on intuitive grounds, and numerical results appear promising.

The explicit treatment of the derived boundary conditions makes them convenient for numerical realization because for the given velocity field at time t, the velocity field at $t + \Delta t$ can be found via solution of the problem with Dirichlet boundary conditions. This velocity field satisfies the incompressibility condition on the artificial boundary as well as in the interior

* Correspondence to: Department of Mechanics and Mathematics, Moscow State University, Moscow 119899, Russian Federation.

Received 28 May 1996
Revised 21 February 1997

of the domain. The considered outflow conditions are local (i.e., differential) in time and space and are readily generalized on a three-dimensional case.

In Section 2, the problem is set up and we argue why the setting of boundary conditions seems natural for simulations of unsteady flows, especially when finite difference (FD) schemes are used.

The test problem modeled is flow in a channel with a damper on the inflow boundary, which moves with some period. The moving damper makes the velocity field substantially unsteady and non-linear, even for moderate Reynolds numbers. Both completely free outflow boundary and one with a forward-facing step are considered.

The numerical scheme for this problem is presented in Section 3. A semi-implicit scheme and a fully coupled solution technique are chosen: the non-linear terms are taken from the previous time step, while viscous and pressure terms are approximated on the current time layer.

Section 4 presents numerical results, and their careful examination, for the problems with various boundary conditions. To give a good idea of the effects of boundary conditions, an 'exact' solution of the problem is computed. Special attention in Section 4 is drawn to:

(i) the solutions behavior near the outflow boundary with different boundary conditions,
(ii) the upstream influence of boundary conditions tested,
(iii) the stability of numerical schemes, and
(iv) the amount of computations in general.

Further remarks and conclusions are given in Section 5.

It should be noted that the methods proposed can be easily transferred to iterative procedures for solving steady problems of fluid dynamics. They are quit suitable also for finite elements, finite volumes and spectral methods for Navier–Stokes equations.

2. SETTING UP OF THE PROBLEM

The momentum equation for two-dimensional viscous incompressible flow can be written in the form [3]

$$\frac{\partial \mathbf{u}}{\partial t} + (\mathbf{u} \cdot \nabla)\mathbf{u} = \nu \nabla^2 \mathbf{u} - \nabla p \tag{1}$$

where $\mathbf{u} = (u_1, u_2)$ is the velocity of flow, $p = p(t, \mathbf{x})$ is the pressure, and ν is the kinematic viscosity.

The incompressibility condition is

$$\operatorname{div} \mathbf{u} = 0 \tag{2}$$

All necessary initial and boundary conditions are determined below.

The computational domain is shown in Figure 1. To make our assumptions clear, we use the notations from Figure 1 below.

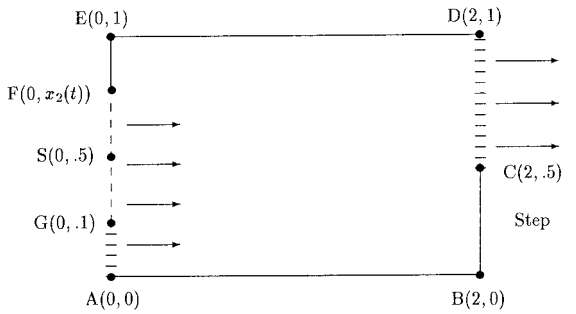

Figure 1. Computational domain.

By segments [AB], [BC], [DE], and [EF] in Figure 1, we denote a boundary with the homogeneous Dirichlet condition $\mathbf{u} = \mathbf{0}$, which has a physical meaning of no-penetration and no-slip of fluid on steady walls. In general, the co-ordinates of point $F = F(0, x_2(t))$ are time-dependent. Here $x_2(t) = x_2(0) + h_F \sin(2\pi K^{-1} t)$, where K is a period of movement, h_F is an amplitude of movement, and $x_2(0)$ is a location of the damper at the initial moment. On the inflow boundary [AF] we set $\mathbf{u} = (\mathscr{P}(x_2), 0)$, where $\mathscr{P}(x_2)$ is a parabolic Poiseuille profile. The flux of the incoming flow is fixed (i.e., $\int_{[AF]} u_1 \, ds = \text{constant} \ \forall t \geq 0$).

The assignment of any 'fixed' boundary condition on the artificial outflow boundary [DC] (i.e., fixed *a priori* flow) turns out to be inadequate. For the proper setting of outflow conditions one can use so-called 'transparent' boundary conditions and related numerical techniques [4–7]. However, for unsteady problems, the transparent boundary conditions are integral in time and space and thus impractical in computations.

The problem of useful local outflow boundary conditions for unsteady, incompressible, viscous non-linear flow appears to be a non-trivial one and has long been a matter of discussion. Here, we include only a brief consideration of several approaches to this problem.

Halpern and Schatzman [1] deduced transparent boundary conditions for Oseen linearization of Navier–Stokes equations. Local absorbing boundary conditions were designed by Halpern and Schatzman as an approximation of the transparent conditions. They can be written in the form

$$\frac{\partial u_1}{\partial t} + (U \cdot \nabla) u_1 = 0 \tag{3a}$$

$$\frac{\partial u_2}{\partial x_1} = 0 \tag{3b}$$

Here and henceforth, $U(\mathbf{x})$ is a known homogeneous 'typical' flow.

Hagstrom [2] constructs asymptotic boundary conditions, which are accurate for dominant wave groups, satisfying spatial Orr–Sommerfeld equations. In vorticity–streamfunction Navier–Stokes calculations these conditions have some success also in the non-linear regime.

Another method, considered by Hagstrom for primitive variables formulation, is the direct application of the scalings used to approximate spatial Orr–Sommerfeld equations. In terms of the physical variables, these are

$$\frac{\partial}{\partial x_1} = O\left(\frac{1}{Re}\right), \qquad \frac{\partial}{\partial t} = O\left(\frac{1}{Re}\right)$$

Using these scalings it is shown that

$$\frac{\partial u_2}{\partial x_1} = O\left(\frac{1}{Re^2}\right) \tag{4a}$$

$$p - \frac{1}{Re}\frac{\partial u_1}{\partial x_1} + C(t) = O\left(\frac{1}{Re^2}\right) \tag{4b}$$

Here, the function $C(t)$ is an arbitrary constant, which may be added to p. Equations (4a) and (4b) result in boundary conditions after dropping the $O(Re^{-2})$ terms. Conditions of this type are quite usual for the Galerkin approach to the Navier–Stokes equations, where appropriate boundary conditions are obtained via specification of a surface traction vector on an artificial boundary. The obtained conditions used to be natural in a weak formulation [8]. For more recent analyses of such an approach see Bruneau and Fabrie [9] and Heywood *et al.* [10].

While conditions (4a) and (4b) are satisfied in a finite element formulation, in a weak sense there direct adaptation for FD methods seems to be questionable. Many (if not most) papers with an FD approach use $\partial(\,\cdot\,)/\partial n$ for normal velocity component. In our model problem it can be the following boundary conditions on [CD]:

$$\frac{\partial u_1}{\partial x_1} = 0, \qquad u_2 = 0 \tag{5a}$$

or

$$\frac{\partial u_1}{\partial x_1} = 0, \qquad \frac{\partial u_2}{\partial x_1} = 0 \tag{5b}$$

If we assume function $\mathbf{u}$ to be smooth enough, then conditions (5a) guarantee the validation of the equality $\operatorname{div}\mathbf{u} = 0$ on the artificial boundary. Sometimes, in order to avoid any 'fixed' conditions on the u_2 component, conditions (5b) are used in practice. However, if one wishes velocity to satisfy conditions (5b), together with the incompressibility equation on the boundary, then the restriction $u_2 = c$ appears again. Moreover, in the above test problem, $c = 0$. However, for unsteady non-linear flow equations, $u_2 = 0$ is not the proper choice on an artificial boundary, apparently.

Note also that the loss of the important conjunction property of $-\operatorname{div}$ and ∇ operators in (5a) and (5b) and the mixed boundary conditions decrease the effectiveness or make it very difficult to use some numerical methods that are good for solving problems of the Stokes- and Navier–Stokes-type with Dirichlet boundary conditions for the velocity function.

Conditions (3a) and (3b) are more convenient for numerical FD realization, since after the explicit time discretization of (3a), one has Dirichlet boundary conditions on $\mathbf{u}\cdot n$ and so the conjunction property of $-\mathrm{div}$ and ∇ can be ensured. Although conditions (3a) and (3b) have theoretical justification in Reference [1] for Navier–Stokes flow, in Section 4 we show that they have evident influence upstream on the flow in the non-linear regime. In this case, Equation (3b) seems troublesome. Note that Equation (3b) appears also as (4a) and as (5b). To avoid this condition for u_2 we use the method of scalings and get $\partial u_2/\partial t = O(Re^{-2})$, $\partial u_2/\partial x_1 = O(Re^{-2})$. Combining these $O(Re^{-2})$ terms results in the following boundary condition:

$$\frac{\partial u_2}{\partial t} + U_1 \frac{\partial u_2}{\partial x_1} = 0 \tag{6}$$

Unlike (3b), Equation (6) has an unsteady nature and could be more suitable for unsteady flows. Beside this, Equation (3a) together with Equation (6) provide us with Dirichlet conditions $\mathbf{u}\cdot n$ and $\mathbf{u}\cdot\tau$ on the outflow boundary after explicit treatment.

In our numerical experiments we formally chose function U through one of the following ways:

(i) $U^{(1)}(\mathbf{x}) = (U_{\text{constant}}, 0)$;
(ii) $U^{(2)}(\mathbf{x}) = (\mathscr{P}(x_2), 0)$, where $\mathscr{P}(x_2)$ is a Poiseuille profile.

Taking into account the proper choice of $U^{(k)}$, Equations (3a) and (6), we can rewrite the outflow boundary conditions for $\mathbf{u}$ in the following way:

$$\frac{\partial \mathbf{u}}{\partial t} + U_1^{(k)} \frac{\partial \mathbf{u}}{\partial n} = \mathbf{0}, \quad k = 1, 2 \tag{7}$$

In view of rather obvious mechanical interpretation, we call boundary condition (7) the *drift conditions*, and function $U(\mathbf{x})$ the *drift function*.

Equations of the transport type were considered on artificial boundaries in various partial differential problems. Conditions similar to Equation (7) were introduced for a two-dimensional wave equation [11] (first-order absorbing boundary conditions) and used on artificial boundaries for wave-like equations [12–14].

Looking for analogs in fluid dynamics theory, we should mention non-reflecting boundary conditions for compressible viscous flow on an artificial boundary [15,16] or their improvement for one-dimensional subsonic flows [17]. It was found that non-reflecting conditions are more effective to reduce a reflection of outflow boundary in contrast to the traditional conditions for pressure. For a treatment of non-linear problems see Hedstrom [16] and Thompson [18]. Ultimately, conditions similar to Equation (7) were mentioned by Gresho [8] as those to be gaining favor (see also Reference [19]). For some other considerations of outflow conditions problem, we also refer to Johanson [20] and Jin and Braza [21].

Let us come back to formula (7). Note that the validity of the equation $\mathrm{div}\,\mathbf{u} = 0$ on the artificial boundary together with conditions (7) does not require any 'fixed conditions on velocity components u_1 or u_2. Only for the stationary solution we obtain $u_2|_{[\mathrm{CD}]} = 0$. In this case, conditions (7) coincide with the conditions of Halpern–Schatzman and 'traditional' (5b).

Existence and uniqueness theorems for the system of equations (1) and (2), the initial data $\mathbf{u}_0(\mathbf{x})$, the boundary conditions (7) on [CD], and the Dirichlet conditions on the other part of boundary hold after time discretization of the system, together with condition (7), i.e., for a known solution at time t and time step τ, functions $\mathbf{u}(t+\tau, \mathbf{x})$ and $p(t+\tau, \mathbf{x})$ are found uniquely. Note that this is *not* the case for conditions (5a) and (5b) or for the stationary problems when no initial conditions are posed (see the counterexample in Reference [19]). The extension of these theorems to the differential case requires additional investigations.

For the sake of convenience we will write the 'fixed' boundary conditions in the form of (7) taking for them $U^{(0)} \equiv 0$. Then, boundary conditions for $\mathbf{u}(\mathbf{x}, t)$ will be the same as boundary conditions for $\mathbf{u}_0(\mathbf{x})$, where $\mathbf{u}_0(\mathbf{x})$ is the initial condition at the moment $t = 0$. For $\mathbf{u}_0(\mathbf{x})$ we take the solution of the stationary Stokes problem with Poiseuille flow on [AS] and [CD].

It should be noted that for very accurate simulation of the flow phenomena, an artificial boundary should be moved 'far' to the right even in the case of absorbing boundary conditions on the outflow. To make the influence of different boundary conditions more clear we do not move away the outflow boundary in our numerical experiments.

Some further remarks on other absorbing boundary conditions of advection type are given in Section 5.

3. NUMERICAL SCHEME

To solve Equations (1) and (2) numerically, we use the staggered grid, which proves to be good enough for the numerical solution of different problems of fluid dynamics [22–25]. Here we describe the numerical scheme used. Let $\bar{\Omega} = [0, 2] \times [0, 1]$, $h_1 = 2/N_1$, $h_2 = 1/N_2$.

Let us introduce the sets

$$\bar{\Omega}_1 = \left\{ \left(\left(i - \frac{1}{2} \right) h_1, j h_2 \right) :\ 0 \le i \le N_1 + 1,\ 0 \le j \le N_2 \right\}$$

$$\bar{\Omega}_2 = \left\{ \left(i h_1, \left(j - \frac{1}{2} \right) h_2 \right) :\ 0 \le i \le N_1,\ 0 \le j \le N_2 + 1 \right\}$$

$$\Omega_3 = \left\{ \left(\left(i + \frac{1}{2} \right) h_1, \left(j + \frac{1}{2} \right) h_2 \right) :\ 0 \le i \le N_1,\ 0 \le j \le N_2 \right\}$$

By $\mathbb{H}_0^h$ we denote a linear space of vector functions defined on $\bar{\Omega}_1 \cup \bar{\Omega}_2$ and vanished on the appropriate grid boundary. Using L^h we denote a space of functions defined on Ω_3, which satisfy the condition

$$\sum_{\mathbf{x} \in \Omega_3} p^h(\mathbf{x}) = 0$$

Operators div^h, ∇^h, $(\nabla^2)^h$ and convective terms $\mathbf{N}(\mathbf{u}^h, \mathbf{v}^h)$ we define the following [23,25]:

$$\operatorname{div}^h \mathbf{u}|_{\mathbf{x}\in\Omega_3} = \sum_{k=1}^{2} h_k^{-1}\left(u_k\left(\mathbf{x}+\frac{h_k}{2}\bar{e}_k\right)-u_k\left(\mathbf{x}-\frac{h_k}{2}\bar{e}_k\right)\right), \quad u\in\mathbb{H}_0^h\cup\mathbb{H}_p^h$$

$$\{\nabla^h p^h|_{(\mathbf{x}^1,\,\mathbf{x}^2)\in\Omega_1\cup\Omega_2}\}_k = h_k^{-1}\left(p^h\left(\mathbf{x}^k+\frac{h_k}{2}\bar{e}_k\right)-p^h\left(x^k-\frac{h_k}{2}\bar{e}_k\right)\right), \quad k=1,2$$

$$N_1(\mathbf{u}^h,\mathbf{v}^h)|_{\mathbf{x}\in\Omega_1} = (4h_1)^{-1}[(u_1^h(\mathbf{x}-h_1\bar{e}_1)+u_1^h(\mathbf{x}))(v_1^h(\mathbf{x})-v_1^h(\mathbf{x}-h_1\bar{e}_1))$$
$$+(u_1^h(\mathbf{x})+u_1^h(\mathbf{x}+h_1\bar{e}_1))(v_1^h(\mathbf{x}+h_1\bar{e}_1)-v_1^h(\mathbf{x}))]+(4h_2)^{-1}$$
$$\left[\left(u_2^h\left(\mathbf{x}-\frac{(h_1\bar{e}_1+h_2\bar{e}_2)}{2}\right)+u_2^h\left(\mathbf{x}+\frac{(h_1\bar{e}_1+h_2\bar{e}_2)}{2}\right)\right)\cdot(v_1^h(\mathbf{x}+h_2\bar{e}_2)-v_1^h(\mathbf{x}))\right.$$
$$\left.+\left(u_2^h\left(\mathbf{x}+\frac{(h_1\bar{e}_1-h_2\bar{e}_2)}{2}\right)+u_2^h\left(\mathbf{x}-\frac{(h_1\bar{e}_1+h_2\bar{e}_2)}{2}\right)\right)(v_1^2(\mathbf{x})-v_1^h(\mathbf{x}-h_2\bar{e}_2))\right]$$

$N_2(\mathbf{u}^h,\mathbf{v}^h)$ is defined similarly. $(\nabla^2)^h$ is the usual five-point approximation of the Laplace operator.

Using the notation $(\alpha\mathbf{I}-(\nabla^2)^h)_0^{-1}\boldsymbol{\psi}$, we denote a solution of the equation $(\alpha\mathbf{I}-(\nabla^2)^h)\mathbf{u}^h=\boldsymbol{\psi}$, $\mathbf{u}^h\in\mathbb{H}_0^h$, where $\mathbf{I}$ is the identity operator, $\alpha\geq 0$ and $\boldsymbol{\psi}$ is defined in all interior nodes of the grid domain.

Further, we use the notations: $\mathbf{u}(\mathbf{x})=\mathbf{u}^h(\mathbf{x},t)$, $\hat{\mathbf{u}}(\mathbf{x})=\mathbf{u}^h(\mathbf{x},t+\tau)$, $p(\mathbf{x})=p^h(\mathbf{x},t)$, $\hat{p}(\mathbf{x})=p^h(\mathbf{x},t+\tau)$, where τ is a time step.

We consider the following scheme. If $\mathbf{u}$ is known already, then the functions $\hat{\mathbf{u}}$ and $\hat{p}$ are determined from

$$\frac{\hat{\mathbf{u}}-\mathbf{u}}{\tau}=\nu(\nabla^2)^h\hat{\mathbf{u}}-\nabla^h\hat{p}-\mathbf{N}(\mathbf{u},\mathbf{u})$$

$$\operatorname{div}^h\hat{\mathbf{u}}=0, \qquad \mathbf{u}^0=\mathbf{u}|_{t=0}$$

$$\hat{\mathbf{u}}|_{\Gamma_0}=0, \qquad \hat{\mathbf{u}}|_{\Gamma_1}=(\mathscr{P}^h(x_2),0)$$

$$\hat{\mathbf{u}}(\mathbf{x})=\theta(\mathbf{u}(\mathbf{x})-\tau h_1^{-1}U^{(k)}(\mathbf{x})(\mathbf{u}(\mathbf{x})-\mathbf{u}(\mathbf{x}-h_1\bar{e}_1))), \quad \mathbf{x}\in\Gamma_2 \tag{8}$$

where Γ_0 is a grid boundary on [AB], [BC], [DE], [EF]; Γ_1 and Γ_2 are grid boundaries on [AF] and [CD] respectively; $\mathscr{P}^h(x_2)$ is a grid projection of the Poiseuille profile; $U^{(k)}\equiv(U^{(k)})^h$ is a grid projection of the drift function, $k\in\{0,1,2\}$; θ is chosen to satisfy the grid analog of the condition $\oint_{\partial\Omega}\hat{\mathbf{u}}\cdot n\,\mathrm{d}s=0$.

Note that $\theta=1$ in the case of free (without the [BC] step) outlet or for the steady solution, generally $\theta\sim 1+c\tau^2$. In the case of $k=0$, we are solving the problem with 'fixed' outflow boundary conditions, and in the case of $k=1,2$, we are solving the problem with the drift conditions on the outlet.

For the Halpern–Schatzman boundary conditions, the equation for u_2 on Γ_2 in Equations (8) is replaced by

$$\hat{u}_2(\mathbf{x}) - \hat{u}_2(\mathbf{x} - h_1\bar{e}_1) = 0, \quad \mathbf{x} \in \Gamma_2$$

On every time step a problem of the Stokes type with parameters should be solved. Consider this problem. After transference of Dirichlet non-homogeneous boundary conditions to the right-hand side of the momentum and compressibility equations, and after elimination of $\hat{\mathbf{u}}$ from these equations, we can rewrite the problem in the following way:

$$\mathrm{div}^h((v\tau)^{-1}\mathbf{I} - (\nabla^2)^h)_0^{-1}\nabla^h\hat{p} = f^h \tag{9}$$

Equation (9) is effectively solved by the conjugate gradient method with the preconditioner [26].

No additional calculations are needed to recover the velocity field $\hat{\mathbf{u}}$. Moreover, $\hat{\mathbf{u}}$ exactly satisfies the incompressibility condition for the accurate solution of (9).

4. NUMERICAL RESULTS

In this section we present and compare results of calculations carried out for the following problems with different outflow conditions (see Figure 1):

(I) The damper [EF] moves up and down with a period of 0.5; the extreme positions of point F are (0, 0.9) and (0, 0.1); $x_2(0) = 0.5$; $\int_{[\mathrm{AF}(t)]} u_1 \, \mathrm{d}s = 1$, $\forall t \geq 0$; all the interval [BD] is considered as the outflow boundary (i.e., point C coincides with B).

(II) The inflow conditions are the same as in the problem I, except on the outlet [BC] the step of height 0.5 is disposed of.

For both problems we also compute a so-called 'exact' solution. For problem I, this is a solution calculated with the outflow boundary moved far to the right ($\bar{\Omega} = [0, 16] \times [0, 1]$, and for problem II this is a solution of the real forward-facing step problem with the step length of 6.

There are a large number of ways to define the Reynolds number $Re = V\ell/v$. For the problems considered it was naturally to choose

$$V = \max_{t \geq 0}\left(|\mathrm{AF}(t)|^{-1} \int_{[\mathrm{AF}]} u_1 \, \mathrm{d}s \right)$$

$\ell = 1$ is the channel height, v is the kinematic viscosity. Thus, we have $Re = 10v^{-1}$.

4.1. On stability of numerical schemes

Using numerical scheme (8) for calculations, one has to keep in mind the conditional stability of this scheme. Restrictions on the time step appear owing to an approximation of the convective terms on the previous time layer. For the sufficient stability conditions of (8) with Dirichlet boundary conditions see Reference [27].

At the same time the discrete analog of drift boundary conditions, which we used (Section 3), can be considered as an approximation of the one-dimensional transfer equation by an explicit, conditionally stable scheme.

Thus, one may expect that the drift boundary conditions could prevent the further loss of stability of the numerical scheme. That is why we turn our attention now to the checking of the stability of numerical scheme (8) for $U^{(1)}$ and $U^{(2)}$.

Numerical experiments were carried out for the problem I. The test below was used to investigate the stability of scheme (8). The numerical scheme was said to be stable if the following relation was valid:

$$\max_{t\in[0,t_1]} \frac{\|\mathbf{u}(t)\|}{\|\mathbf{u}(0)\|} \leq M$$

where $t_1 = 10K$, $M = 100$, $\|\cdot\|$ is the L_2 norm.

In Table I one can see values of maximum τ, for which numerical scheme (8) is stable in the above sense.

The values of τ from Table I were found through the dichotomy method for solving the problem $\chi(\tau) = 0.5$ with the aspect error 0.001, where

$$\chi(\tau) = \begin{cases} 0, & \text{if the problem is not stable} \\ 1, & \text{if the problem is stable} \end{cases}$$

Symbol * in Table I means that for different initial values of τ, the calculated results differ and lie in the interval [0.00014, 0.00025]. This effect indicates irregular behavior of the function χ near the point of stability loss for numerical scheme with $U^{(0)}$, $v = 5 \times 10^{-4}$.

We can see from Table I that restrictions on the time step, which we have to introduce to guarantee stability, are not stronger for the drift conditions $U^{(1)}$ and $U^{(2)}$ than for 'fixed' boundary conditions ($U^{(0)}$), and they are slightly weaker for higher Re.

The above criterion does not guarantee that exponential instability is suppressed for all τ calculated. This criterion is used only for comparison. However, the calculated values of τ are very close to critical. In Figure 2 we show the evolution of the solution through time with

Table I. Critical τ for stability of scheme grid 32×64, $Re = 10v^{-1}$, $t_1 = 5$.

$v \backslash U$	U^0	U^1	U^2
0.03	0.00631	0.00631	0.00631
0.01	0.00100	0.00100	0.00100
0.001	0.000263	0.000293	0.000269
0.0005	*	0.000148	0.000124

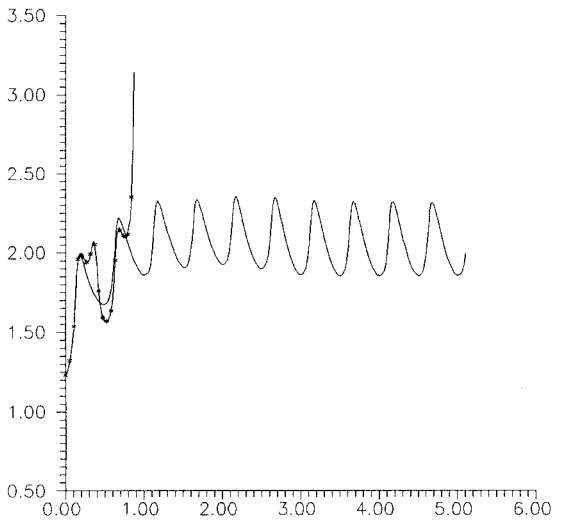

Figure 2. Behavior of velocity spatial norms for $\tau = 0.001$ and $\tau = 0.00105$.

$\nu = 0.01$, U^2, $\tau = 0.00105$ and $\tau = 0.001$. For $\tau = 0.00105$ the solution blows up and for $\tau = 0.001$ calculations are stable. The solutions of the problem for $\tau = 0.001$ and for $\tau = 5 \times 10^{-4}$ that guarantee stability of the scheme were in a very good agreement.

4.2. On accuracy of numerical schemes

While results on accuracy of the marker and cell (MAC) scheme are well known (see Reference [28]) and the use of this scheme in computational fluid dynamics has a long history, its application with given data requires additional checking of convergence. To this end, the 'exact' solution of problem I was calculated on four embedded grids, with $h = 1/16$, $1/32$, $1/64$, and $1/128$ respectively, and other data fixed, in particular $\nu = 0.01$. Pointwise convergence was detected both for pressure and velocity; see Figure 3 as an illustration for two points. Solutions for $h = 1/64$ and $h = 1/128$ practically coincide. A minor loss of convergence in pressure is due to the well-known lack of regularity for pressure function in comparison with velocity. The grid with $h = 1/64$ was chosen for our further calculations.

4.3. General form of solution, influence of boundary conditions

Calculations were performed with $\nu = 0.01$ ($Re = 10^3$), and the time interval equal to $20K$, where $K = 0.5$ is the period of damper movement. Setting $\tau = 2 \times 10^{-4}$ to reach the stability of the numerical scheme (Table I), we obtain solutions of the problem with the drift boundary

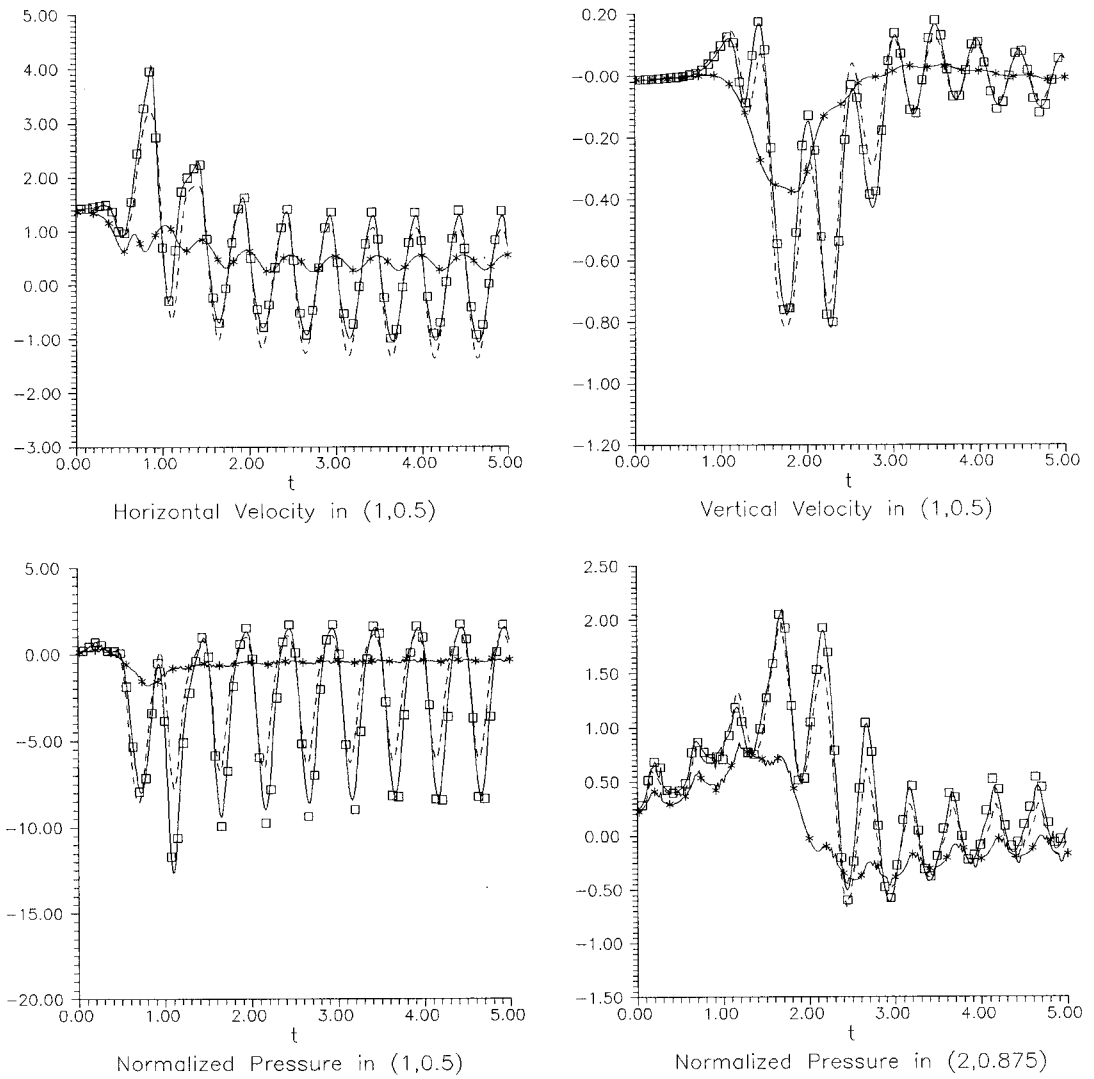

Figure 3. Time histories of u_1, u_2 and p in point (1, 0.5) and p in (2, 0.875), where $- * -$, $h = 1/16$; $- - -$, $h = 1/32$; —, $h = 1/64$; $-\square-$, $h = 1/128$.

conditions ($U^{(k)}$, $k = 0, 1, 2$), Halpern–Schatzman (HS) boundary conditions, and the 'exact' solution on time interval $[0, 20K]$. A solution of the stationary Stokes problem was considered as the initial value; therefore, the further evolution of the flow can be divided into two qualitatively different stages

(I) the stage of periodic solution formation
(II) the stage of periodic behavior of the solution

The duration of the first stage can be estimated approximately as $4K$ (or ~ 2). For the outflow boundary without the [BC] step, the typical behavior of the flow is demonstrated in Figures 4–8 (we show streamlines for not-time-average data).

At first the single vortex is formed behind the damper. Since the damper goes down and the average inflow velocity increases, the intensity of the vortex is growing and its center is moving down.

Sufficiently large Reynolds number and small period K provide separation of this vortex when the damper goes up; after separation, the vortex drifts downstream. Here, the general form of solutions for all considered problems is the same (Figure 4).

On time interval from 0.5 up to 1.0, the form of solutions for different boundary conditions is also practically the same and is shown in Figure 5. Here, as well as on every period of damper movement, the large vortex is forming behind the damper with its further progress downstream. These large vortices are said to be 'main'.

Along the bottom wall, the bending streamlines form a new smaller eddy, recirculating in the opposite direction as that within the main vortex. Further, the formation and downstream progress of the smaller secondary eddy along the bottom wall happen at every period of damper movement. Formation of these downstream moving eddies for the transitional and turbulent regimes in a channel with a backwards-facing step is reported in Reference [29].

Beginning with time $2K$, differences in the flow behavior for various boundary conditions become appreciable (Figures 6–8). Most of all, differences in the behavior of the secondary eddy along the bottom wall are noted. Thus, in the case of 'fixed' boundary conditions (Figure 6), the eddy decays after reaching the artificial boundary; in the case of uniform drift conditions (drift conditions with $U^{(1)}$) (Figure 7), the eddy passes over the artificial boundary unnaturally increasing; finally, in the case of Poiseuille drift conditions (with $U^{(2)}$) (Figure 8), the eddy also passes over the boundary with a less increase. In the latter case, the solution coincides with the 'exact' one.

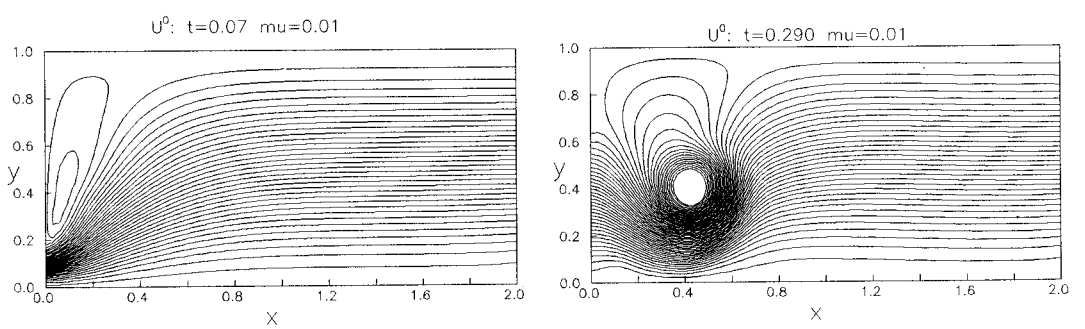

Figure 4. The main vortex is forming and moving downstream.

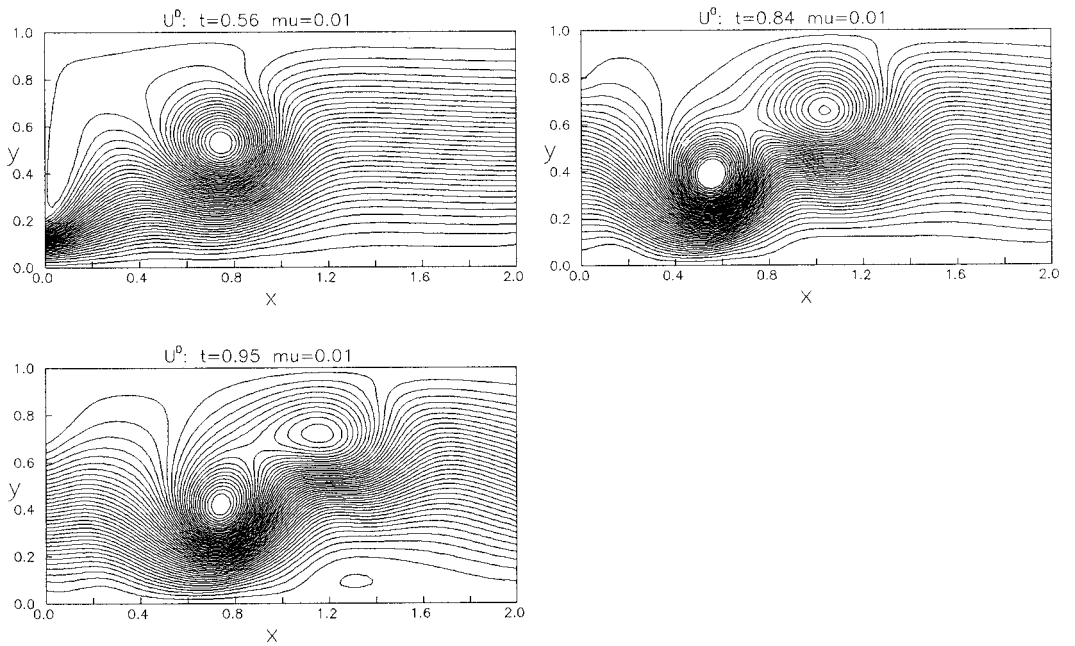

Figure 5. Formation of the secondary eddy along the bottom wall and of the next main vortex.

Let us turn to the description of the solution during the second stage, the stage of the periodic solution behavior (Figures 9–13); we consider time $4K$ as the beginning of this stage. Now the flow near outflow boundary is substantially unsteady and non-linear. Here we compare solutions in the case of HS boundary conditions and drift boundary conditions with the 'exact' solution. In all these cases, on every time interval of K, only one main vortex forms and disappears. Thus, two or three main vortices are observed simultaneously during the period of damper movement.

Further we focus our attention on the peculiarity of the main vortices evolution with different outflow conditions. The 'exact' solution is shown in Figure 9. The main vortices moving in the direction of top right corner of the domain are observed. Changes in the form of the main vortex near the outflow boundary are caused by the influence of the previous vortex which has already passed over the boundary.

In the case of 'fixed' boundary conditions (drift function: $U^{(0)}$) (Figure 10), the main vortex dissipates after reaching the corner, staying immovable. Similarly, after some growing, the secondary eddy decays in the bottom right corner.

In the case of uniform drift boundary conditions, the main vortex passes smoothly over the outflow boundary (Figure 11). The secondary eddy passes over the artificial boundary along the bottom wall without visible changes of size.

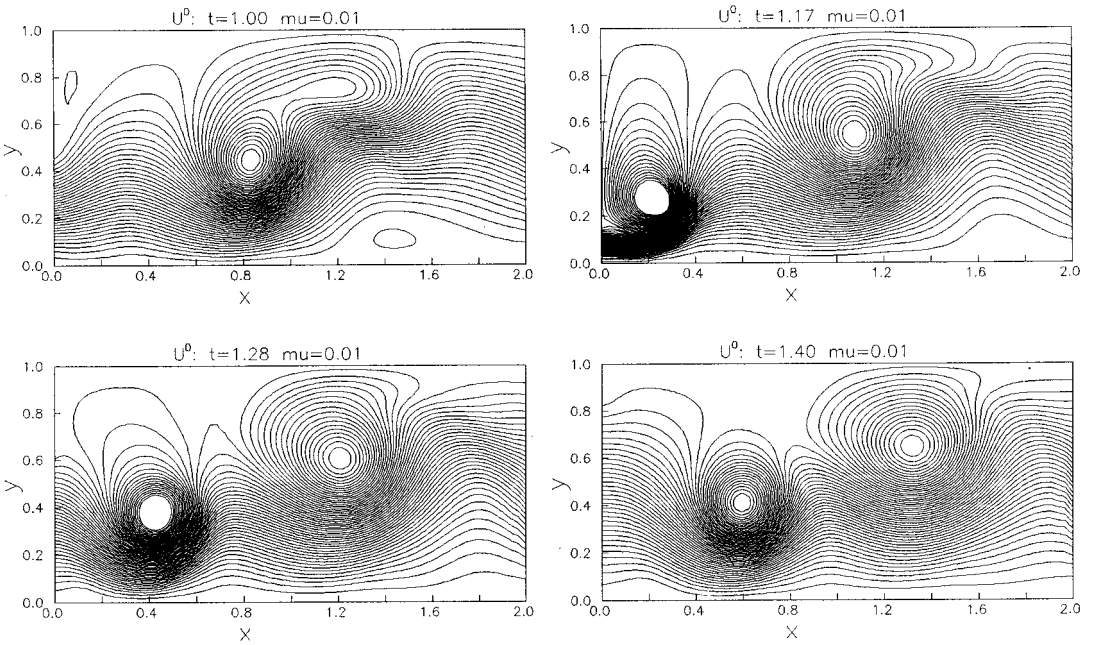

Figure 6. The decay of the secondary eddy, 'fixed' boundary conditions.

In the case of Poiseuille drift conditions (Figure 12) and HS conditions (Figure 13), the situation does not change substantially in comparison with uniform drift conditions. However, in the both cases of drift boundary conditions and in the case of HS conditions, the main vortex undergoes some distortion passing the outflow boundary. So far a preference can not be made and further study and comparison are performed below.

Thus, for Problem I we see that in the cases of the drift conditions $U^{(k)}$, $k = 1, 2$, and HS conditions, a more reliable situation of fluid motion in comparison with 'fixed' conditions is observed. The latter are improper and have influence on the flow far upstream. Differences in the solutions behavior for two drift conditions settings are also seen. During the first stage, the shape of the secondary eddy, passing over the outflow boundary, is more reliable for the Poiseuille drift conditions.

Evidently, the proper boundary conditions should minimize the upstream influence of the artificial boundary, i.e., the error introduced by setting some conditions on the artificial boundary should be localized near this boundary. In Figures 14 and 15 the difference in pressure between the 'exact' solution and solutions with all tested boundary conditions is shown for $y = 0.5$ (center of domain) and $y = 0.94$ (near the top wall). Here we plot an aspect error, i.e., the difference divided by the appropriate L_2 norm of the 'exact' solution. We see that drift conditions with $U^{(1)}$ and HS conditions, as well as 'fixed' boundary conditions, may produce spurious oscillations in pressure far upstream. Moreover, 'fixed' boundary conditions

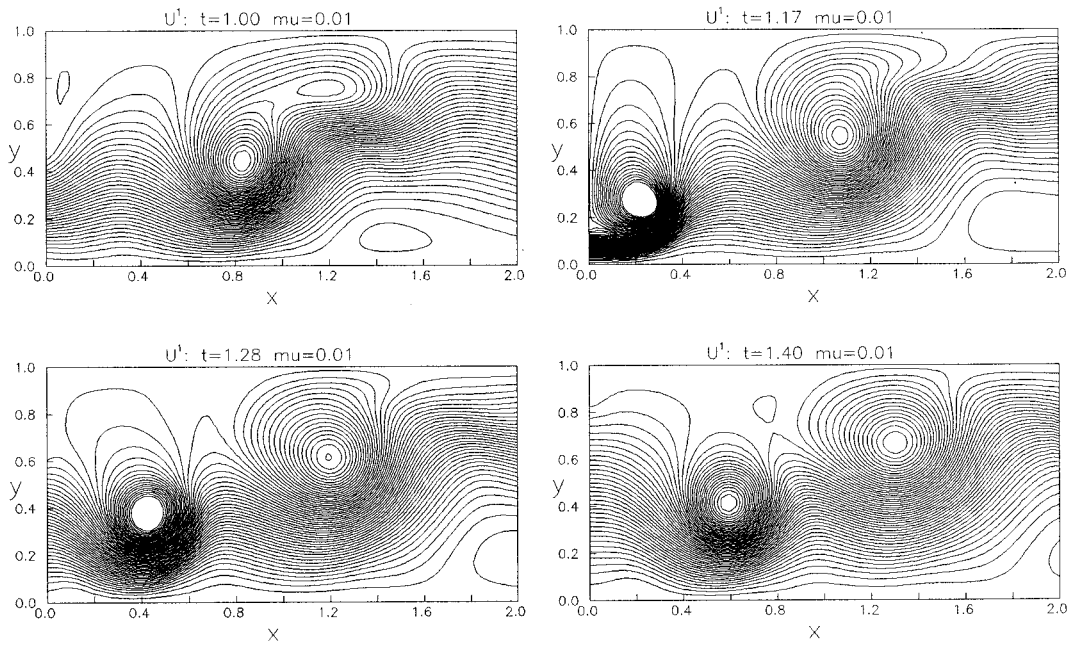

Figure 7. Passing of the secondary eddy over the boundary with uniform drift conditions.

cause a dramatic growth in error near the artificial boundary ($t = 3.8$, $t = 3.9$ in Figure 14 and $t = 3.5$, $t = 4.0$ in Figure 15). Only the drift boundary conditions with the Poiseuille drift function (U^2) demonstrate a decay of oscillations in error function in some region near the artificial boundary. Note also that the error in pressure is defined in each time up to an additive constant (as well as pressure functions themselves).

A similar situation is observed for the difference in u_1 (Figure 16) and u_2 (Figure 17) between the 'exact' solution and solutions with various boundary conditions ($y = 0.5$ in both cases). Again the drift boundary conditions with U^2 demonstrate the best results. Note that the HS boundary conditions produced sometimes better results upstream than the 'fixed' conditions ($t = 3.8$, $t = 3.9$ on Figure 16 and $t = 3.5$–3.7 on Figure 17).

Now we turn our attention to the behavior of different flow characteristics on the artificial boundary. In Figure 18 the profiles of the u_1 velocity component on the outflow are shown. The u_1 profiles in the cases of the Poiseuille drift conditions and HS conditions practically coincide and they are in a better agreement with 'exact' conditions than with profiles of the solution with uniform drift conditions.

In Figure 19 the profiles of u_2 velocity on the outflow are shown. For all boundary conditions, the u_2 component on the outflow is rather far from the 'exact' one and no

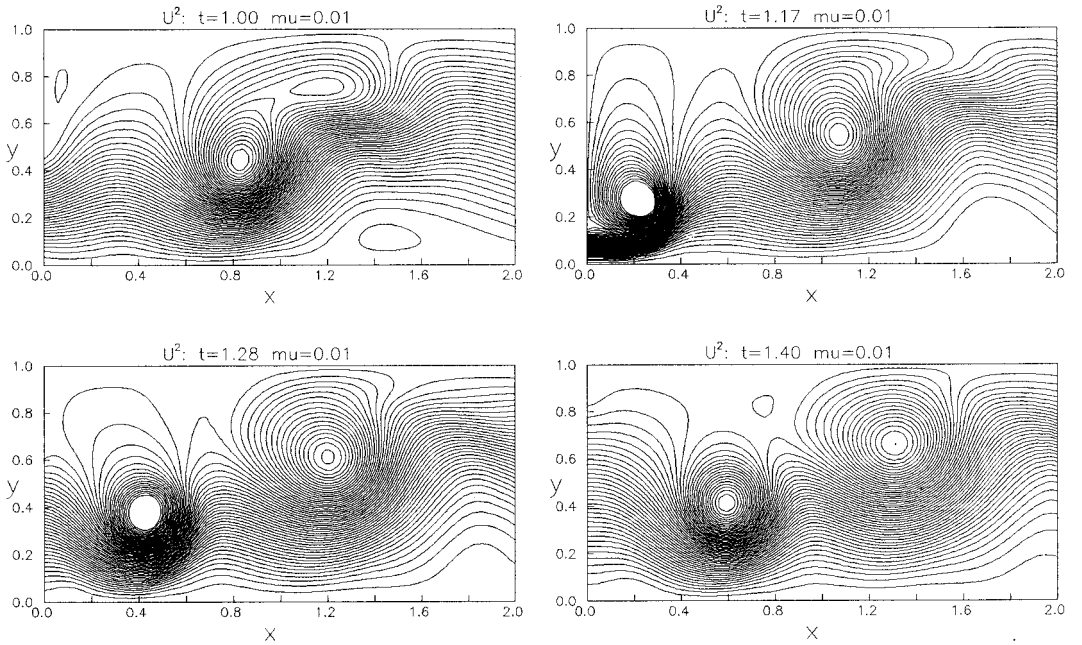

Figure 8. Passing of the secondary eddy over the boundary with Poiseuille drift conditions.

preference could be given. It seems that the observation of velocity profiles on the artificial boundary helps us to explain the success of the Poiseuille drift conditions in comparison with uniform drift conditions, but not yet with HS conditions. This is why we also compare the normal derivatives of velocity components on the outflow.

In Figure 20 we show $\partial u_1/\partial n$ on the outflow. For the Poiseuille drift conditions and HS conditions, the results are the same and only qualitatively correspond to the 'exact' derivatives for some t.

In Figure 21 we show $\partial u_2/\partial n$ on the outflow. We recall that $\partial u_2/\partial n = 0$ for HS conditions, and from Figure 21, we see that this condition is too far from being satisfied by the 'exact' solution. It seems that the drift boundary conditions with U^2 and even with U^1 produce a better approximation of $\partial u_2/\partial n$ on the outflow than HS conditions. We propose that the success of the Poiseuille drift conditions is due to the better approximation of the normal derivative of u_2 in comparison with $\partial u_2/\partial n = 0$. For the 'fixed' boundary conditions, the values of $\partial u_1/\partial n$ and $\partial u_2/\partial n$ are absolutely wrong.

Now we will present some results for Problem II. In Figures 22–25 we show the full period of problem II solutions (i.e., with the [BC] step on the outflow), the exact one (Figure 22) and with various boundary conditions.

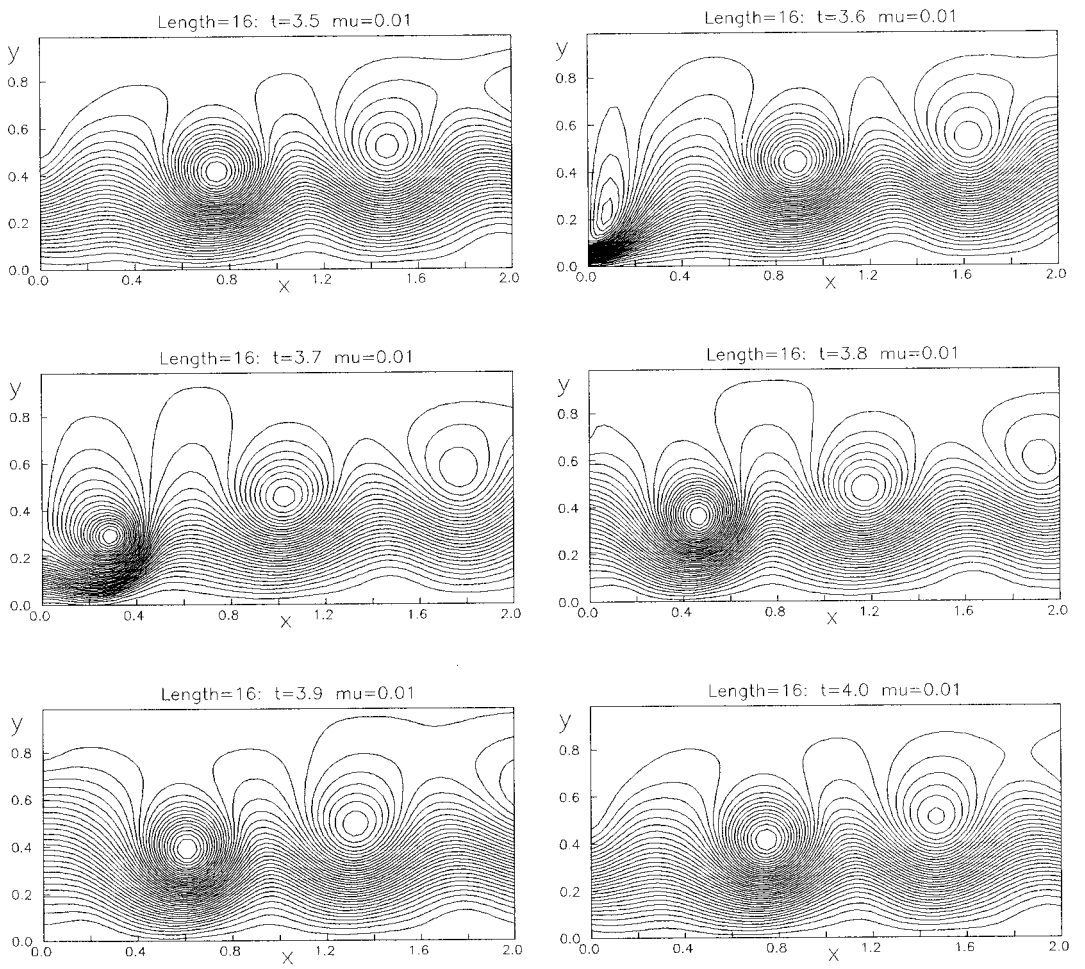

Figure 9. The 'exact' solution; restriction of the elongated computational domain.

As well as in Problem I, we carried out our calculations on time interval $[0, 20K]$ with $\tau = 2 \times 10^{-4}$, $\nu = 0.01$. After $4K$, solutions have a periodic behavior. Now the secondary eddy, moving along the bottom wall, does not approach the outflow boundary, but flowing together with the small eddy at the base of the [BC] step, leads to its pulsation.

For the 'fixed' boundary conditions (Figure 23), just as in Problem I, a gradual decay of the main vortex is observed in the top right corner of the domain.

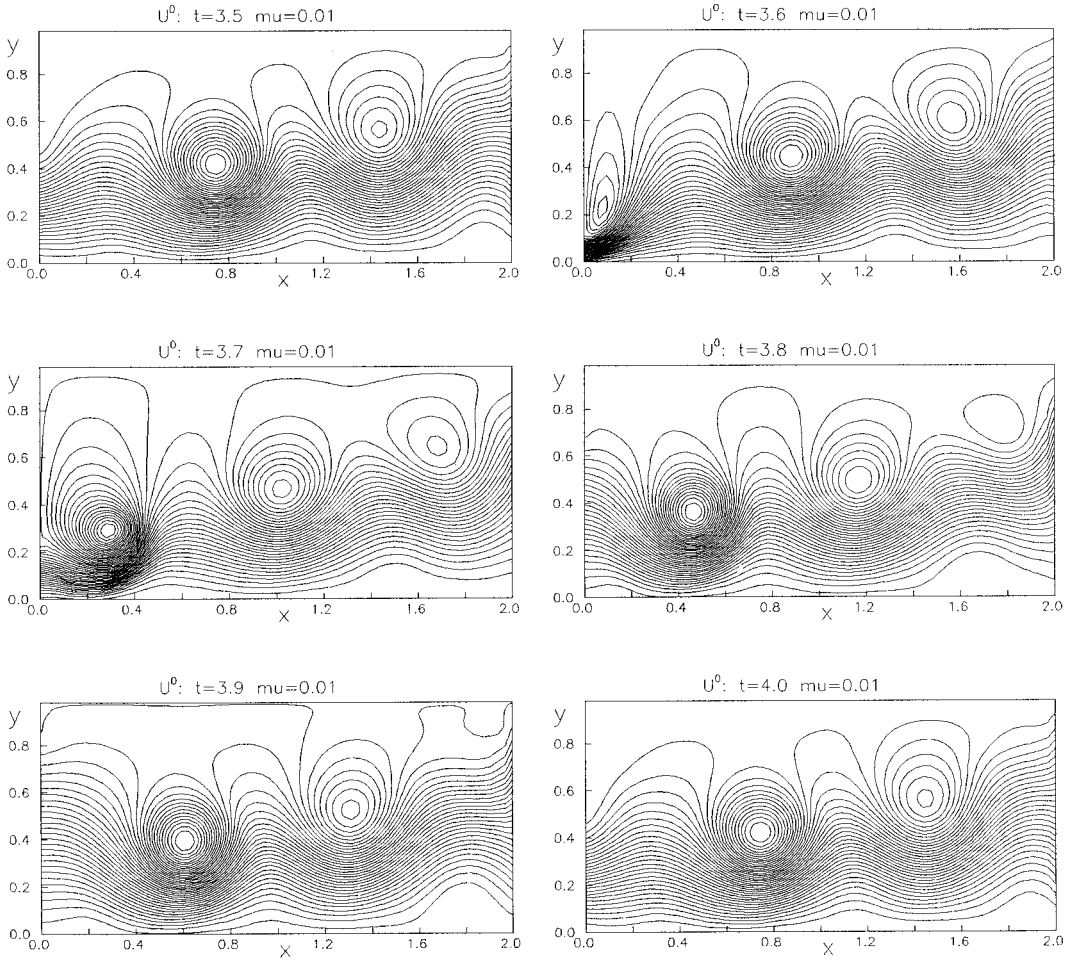

Figure 10. The decay of the main vortex, 'fixed' boundary conditions.

For the uniform drift boundary conditions, the main vortex decreases and passes smoothly over the outflow boundary (Figure 24). The behavior of the flow near the artificial boundary is qualitatively the same as in the 'exact' case.

For the Poiseuille drift boundary conditions (Figure 25), the situation seems to differ from the case of the uniform drift: the main vortex moves to the top right corner, where it distorts and dissipates. However, in contrast to the 'fixed' boundary conditions, no spurious oscillations are observed near the outflow.

Thus, in Problem II only the uniform boundary conditions turn out to be acceptable in the sense of mechanical reliability of the solution obtained. The uniform boundary conditions

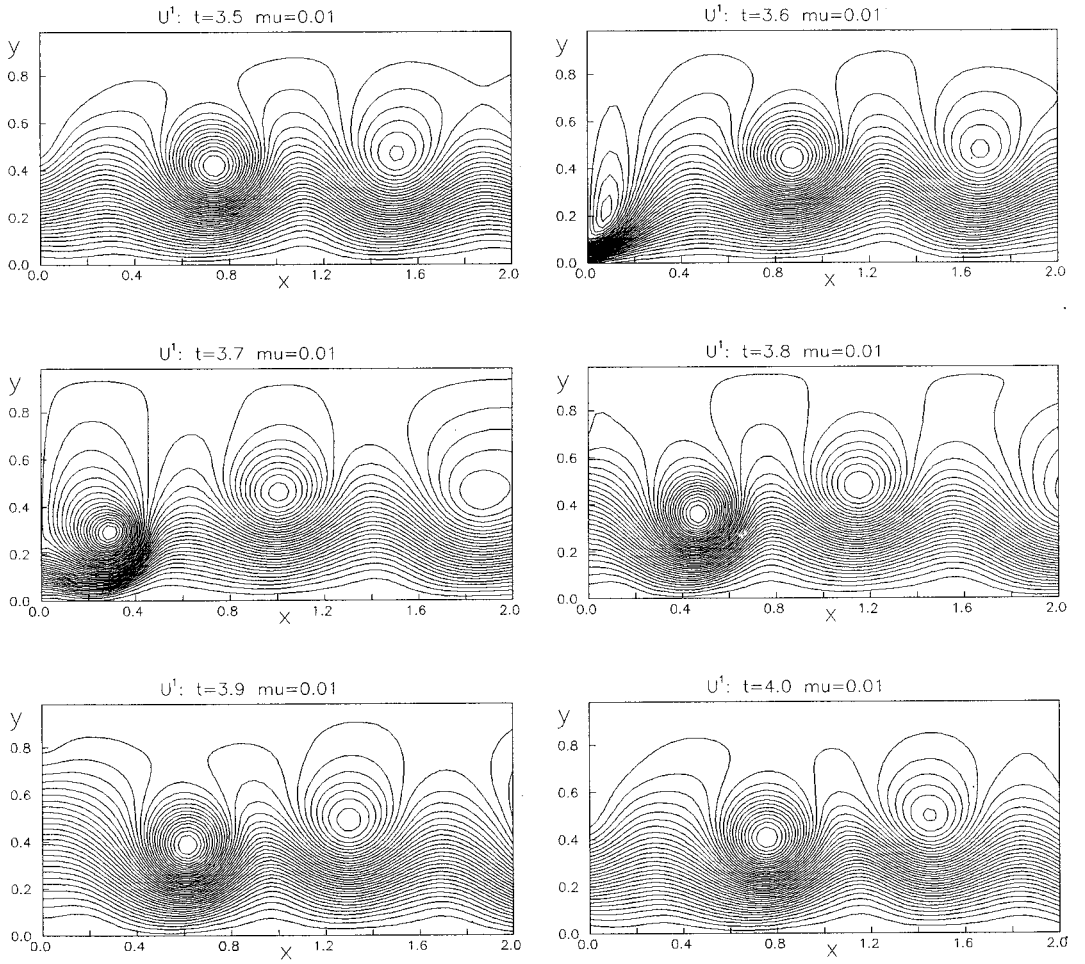

Figure 11. Passing of the main eddy over the boundary with uniform drift conditions.

appear probably to be the most preferable, when a 'typical' flow U (see Section 2) cannot be distinguished on the outflow boundary.

In Figure 26 we demonstrate the difference in pressure between the 'exact' solution and solutions with the drift boundary conditions U^k, $k = 0, 1, 2$ for $y = 0.75$. All boundary conditions have approximately the same upstream influence.

4.4. On computational inputs

To give a quantitative idea of the computational inputs we present in Table II the CPU time needed for some problems considered.

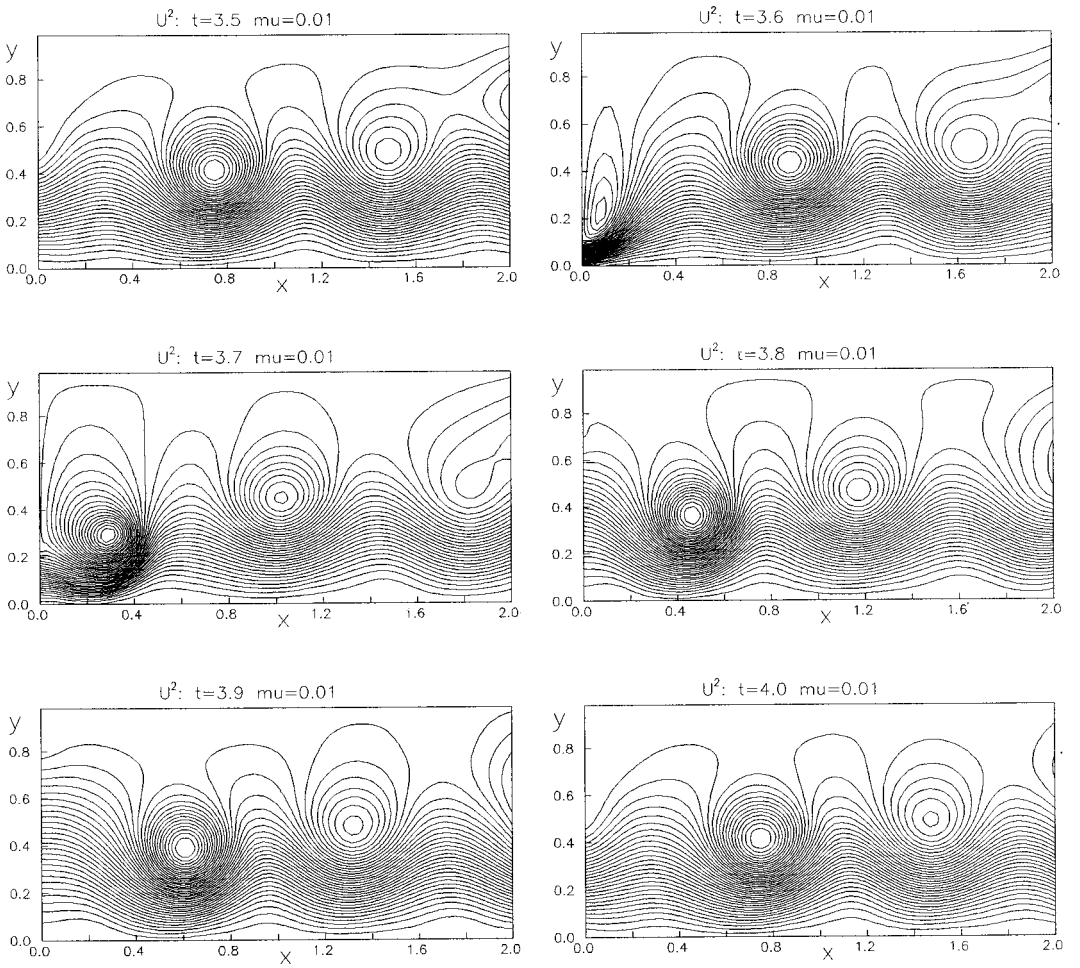

Figure 12. Passing of the main eddy over the boundary with Poiseuille drift conditions.

Almost the same CPU time for the problems with various boundary conditions (other parameters are fixed) indicates that norms of solution differences on neighboring time layers have approximately the same ratio and the cost of one time step was the same for all considered boundary conditions.

Note that the 2.5-times increase in the number of time steps and 2-times increase in the number of grid points provided only a 2.4-times increase in CPU time. It can be explained, firstly, by the 2-times reduction in norms of solutions' differences on neighboring time layers

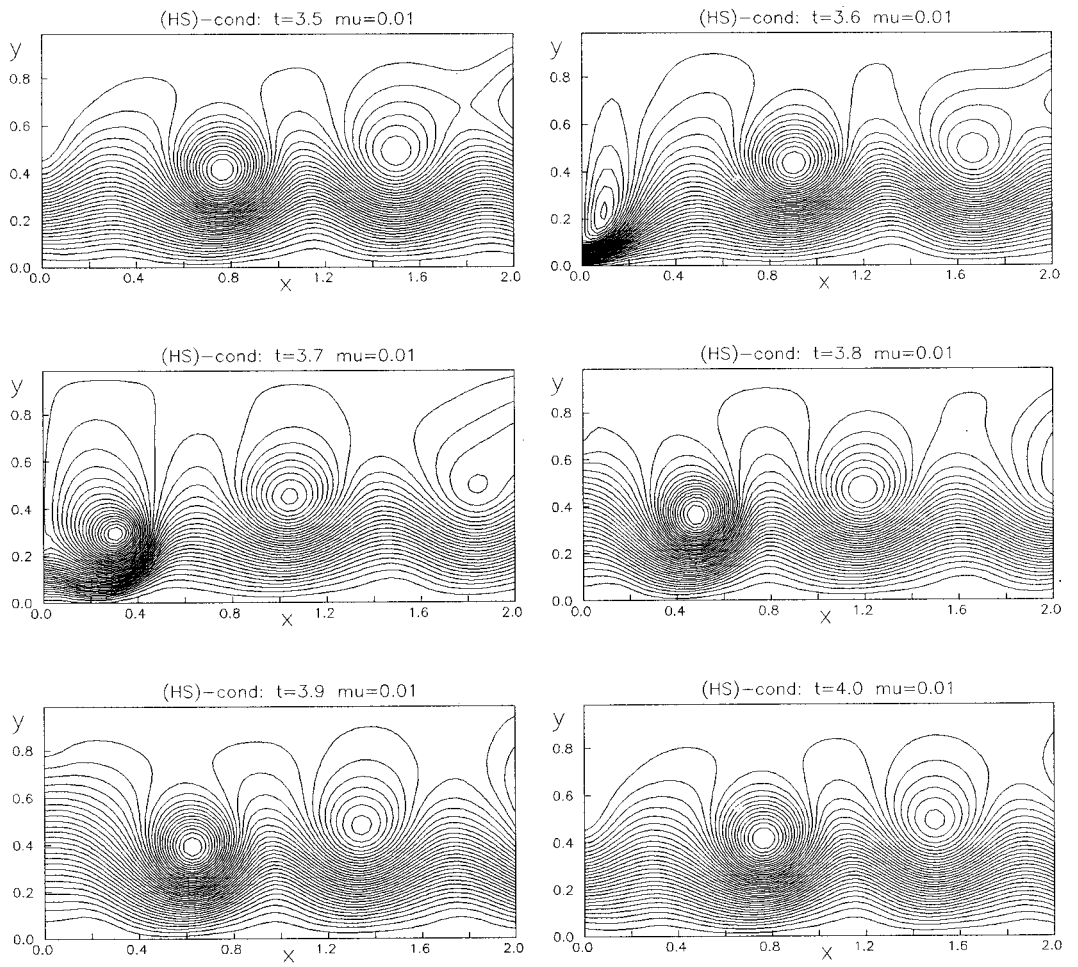

Figure 13. Passing of the main eddy over the boundary with HS boundary conditions.

and, secondly, decreasing of τ (as well as ν) implies growth of convergence rate of the interior iterative process used (see Section 3 and Reference [26]).

5. REMARKS AND CONCLUSIONS

Much more various combinations of velocity components and their derivatives can be considered on the artificial boundary as an outflow condition. Many of them can be found in

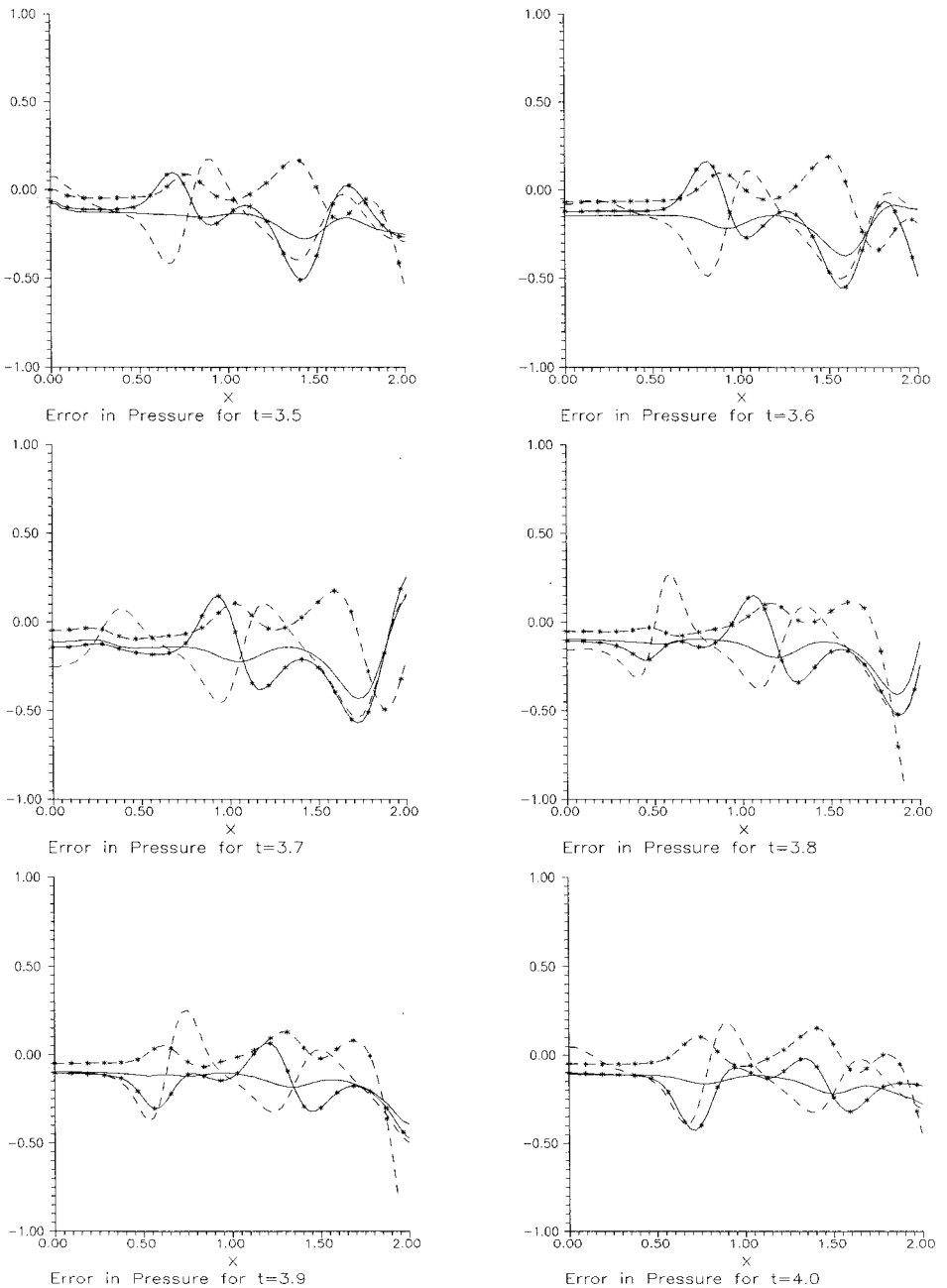

Figure 14. Error in pressure for $y = 0.5$, where – ∗ –, b.c. with U^0; -×-, b.c. with U^1; —, b.c. with U^2; – – –, HS b.c.

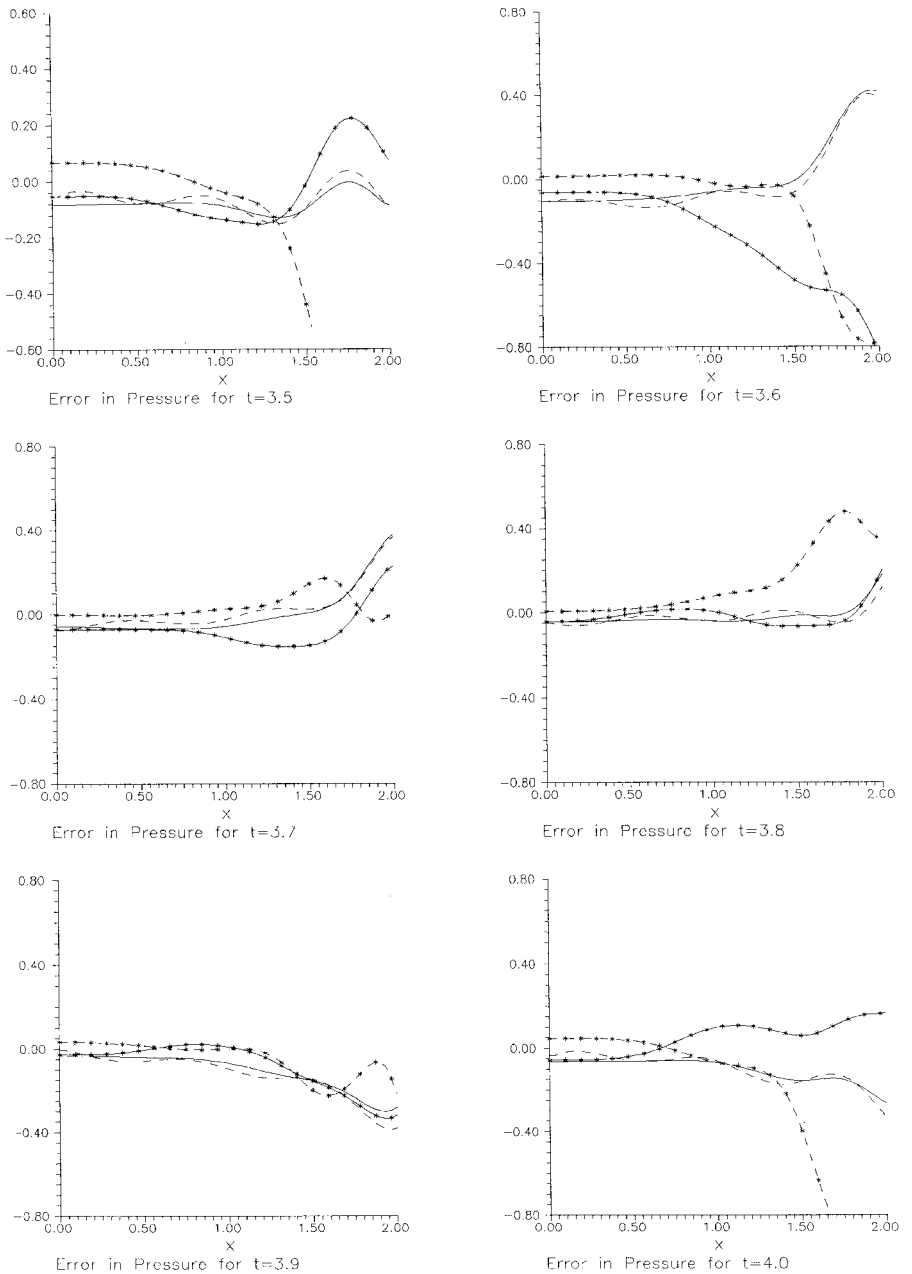

Figure 15. Error in pressure for $y = 0.94$, where – ∗ –, b.c. with U^0; -×-, b.c. with U^1; —, b.c. with U^2; – – –, HS b.c.

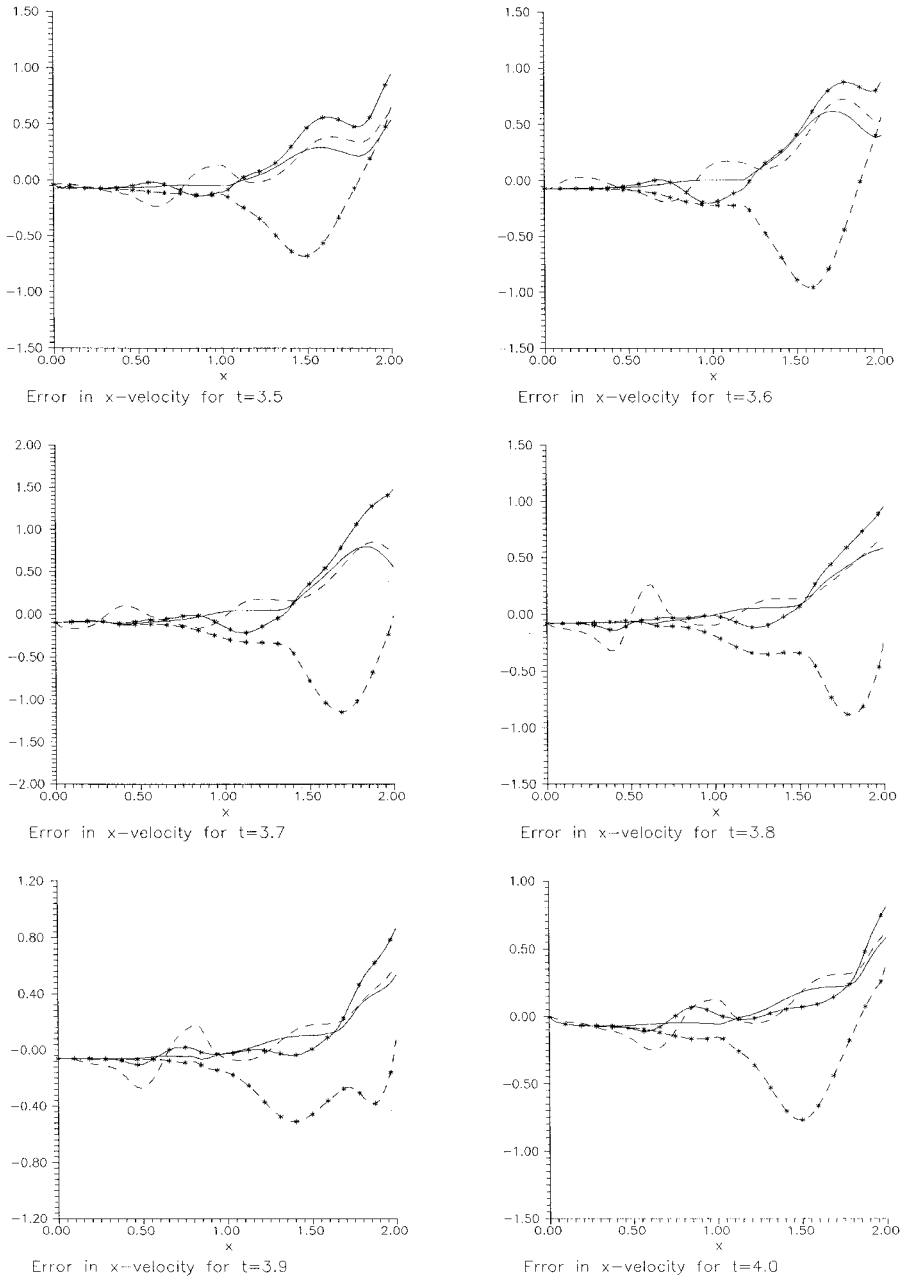

Figure 16. Error in u_1 for $y = 0.5$, $- * -$, b.c. with U^0; $-\times-$, b.c. with U^1; —, b.c. with U^2; $- - -$, HS b.c.

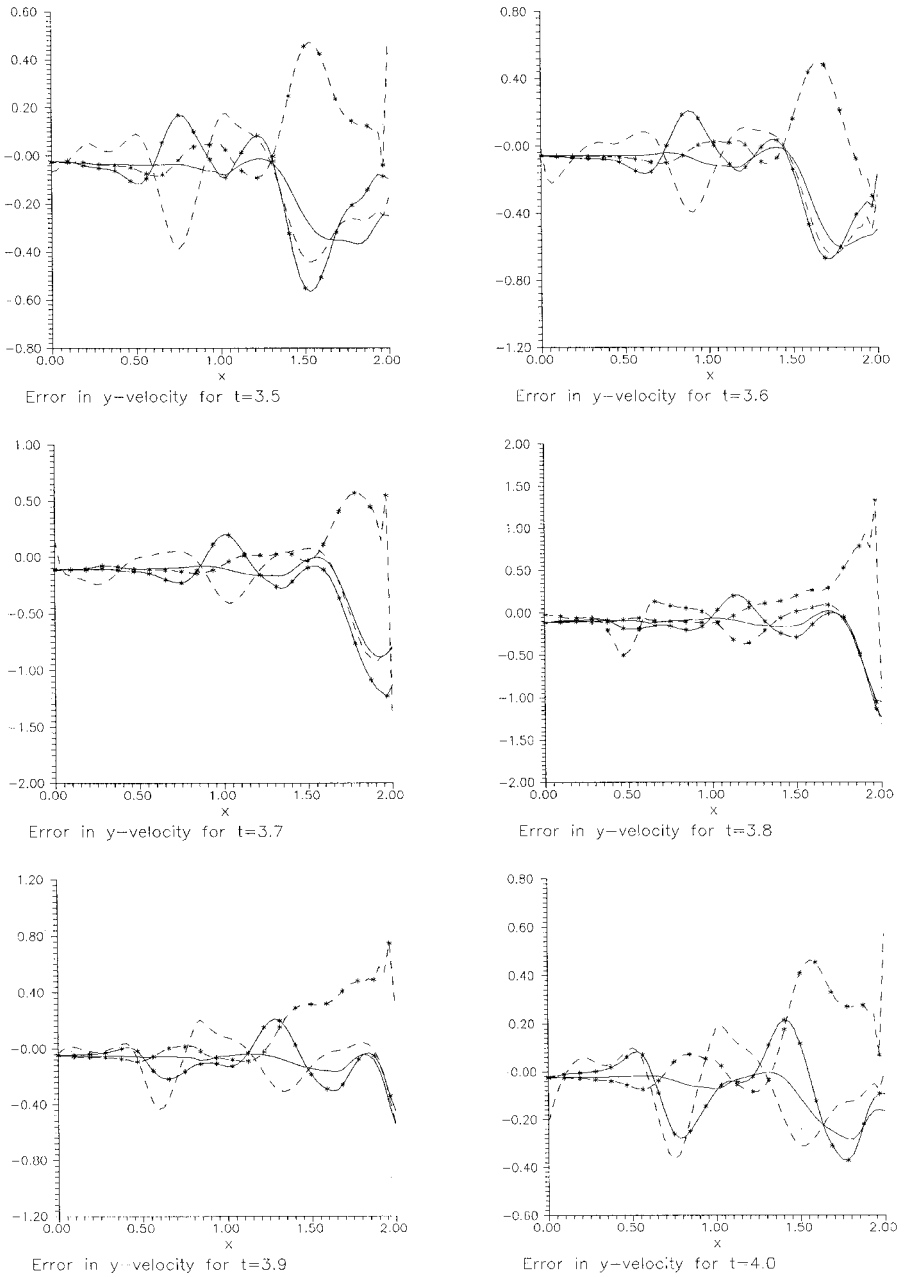

Figure 17. Error in u_2 for $y = 0.5$, where $- * -$, b.c. with U^0; $-\times-$, b.c. with U^1; —, b.c. with U^2; $- - -$, HS b.c.

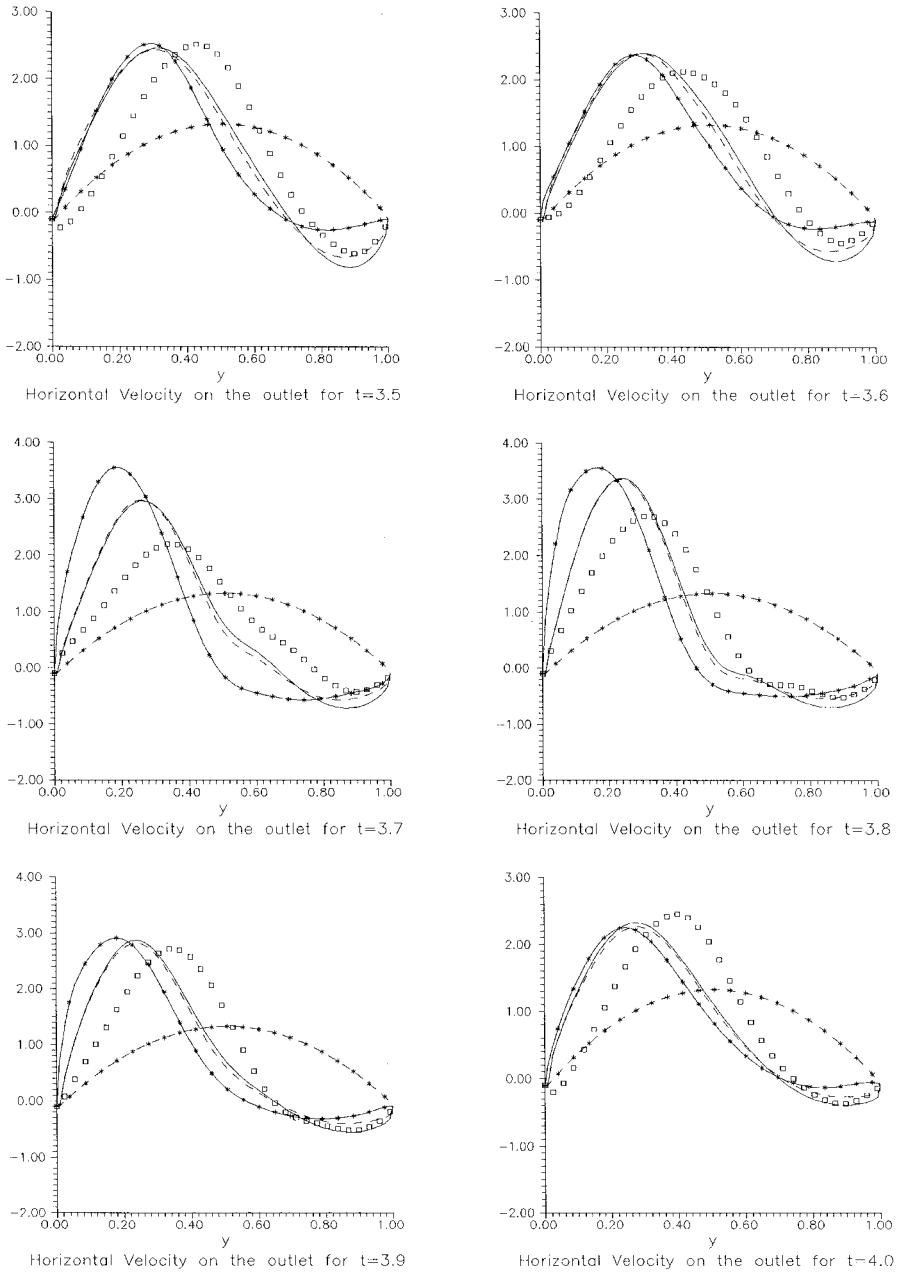

Figure 18. u_1 profile on the outlet ($x = 2$), where □, exact; – ∗ –, b.c. with U^0; -×-, b.c. with U^1; —, b.c. with U^2; – – –, HS b.c.

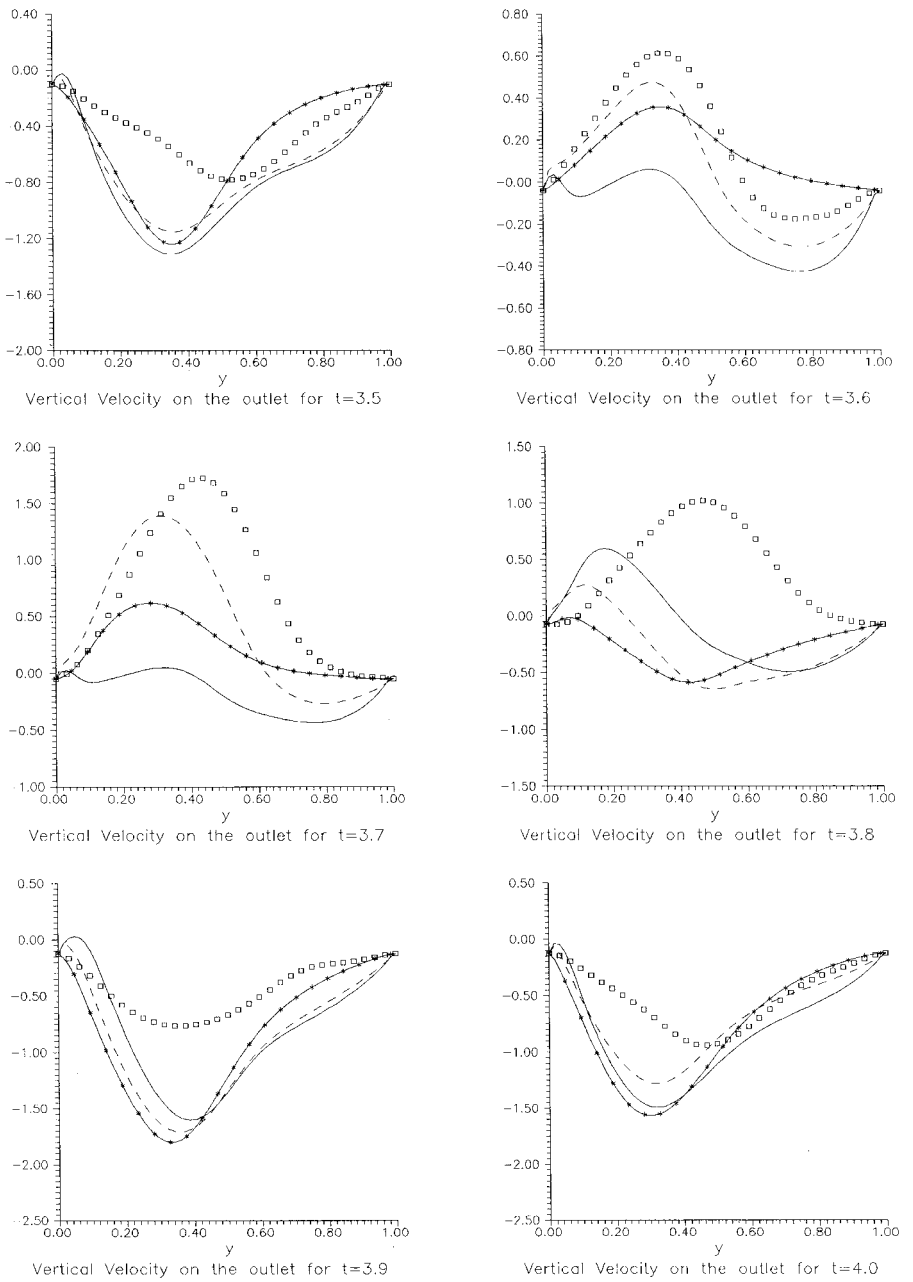

Figure 19. u_2 profile on the outlet ($x = 2$), where □, exact; – ∗ –, b.c. with U^0; -×-, b.c. with U^1; —, b.c. with U^2; – – –, HS b.c.

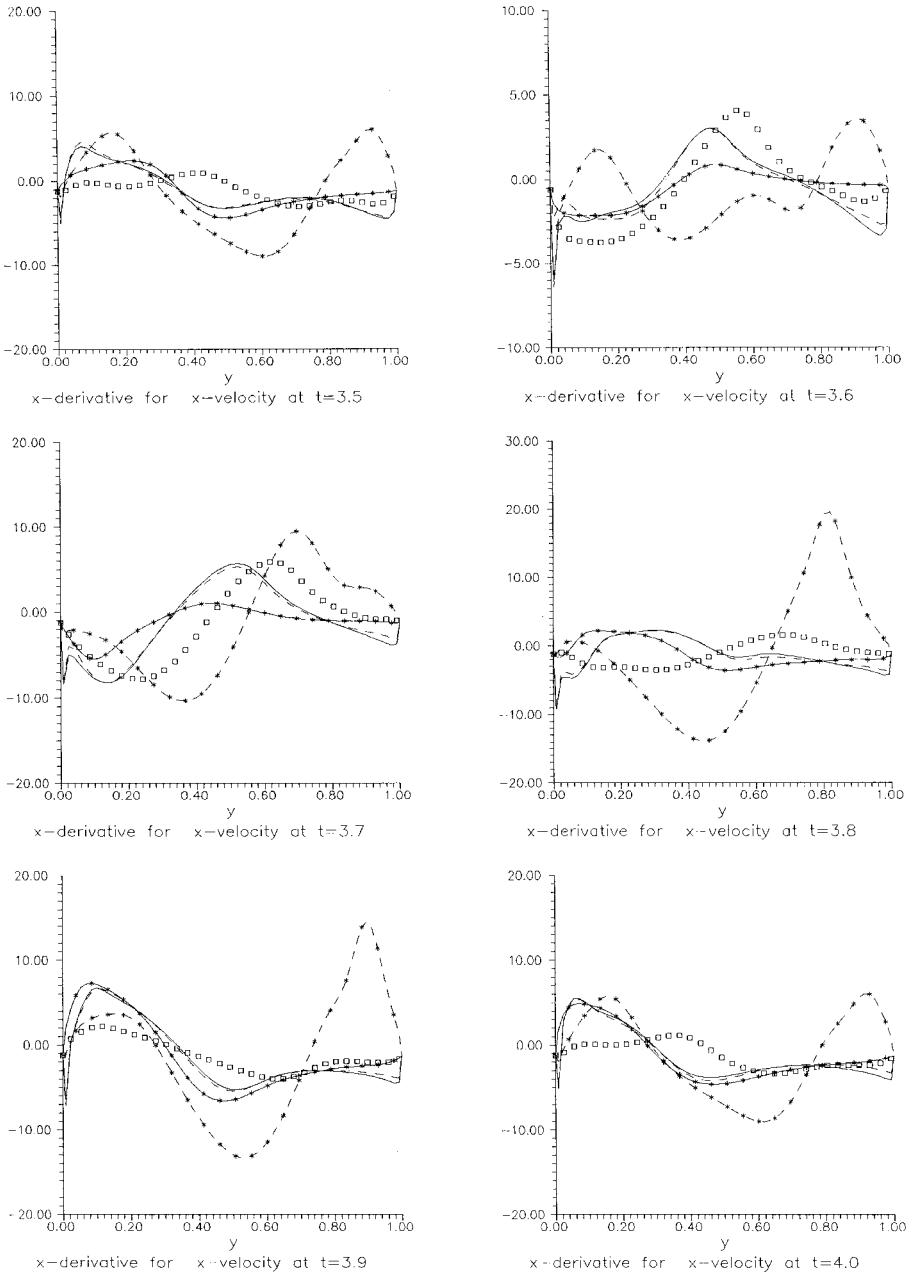

Figure 20. $\partial u_1/\partial x$ on the outlet ($x = 2$), where □, exact; – ∗ –, b.c. with U^0; -×-, b.c. with U^1; —, b.c. with U^2; – – –, HS b.c.

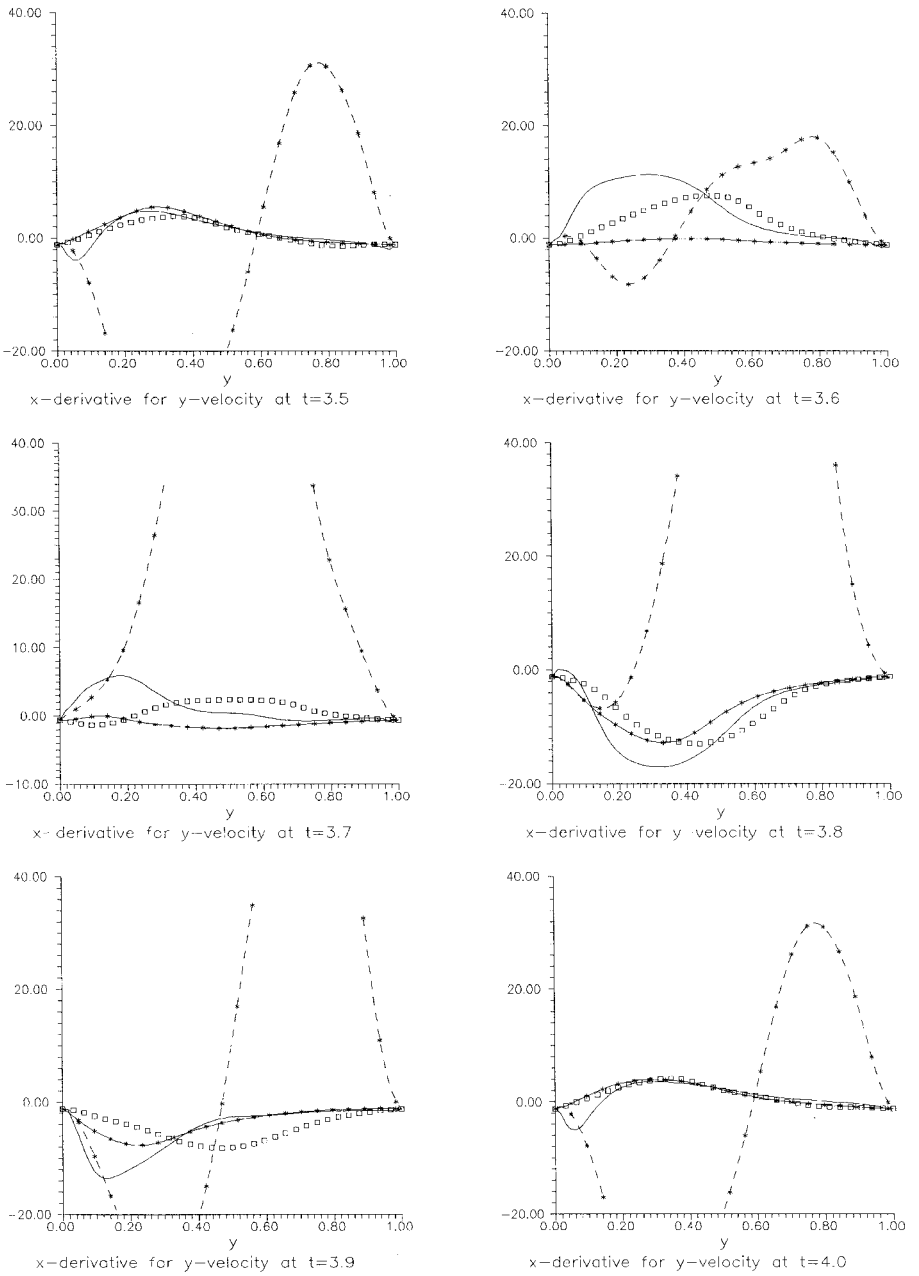

Figure 21. $\partial u_2/\partial x$ on the outlet ($x = 2$), where □, exact; – ∗ –, b.c. with U^0; -×-, b.c. with U^1; —, b.c. with U^2; – – –, HS b.c.

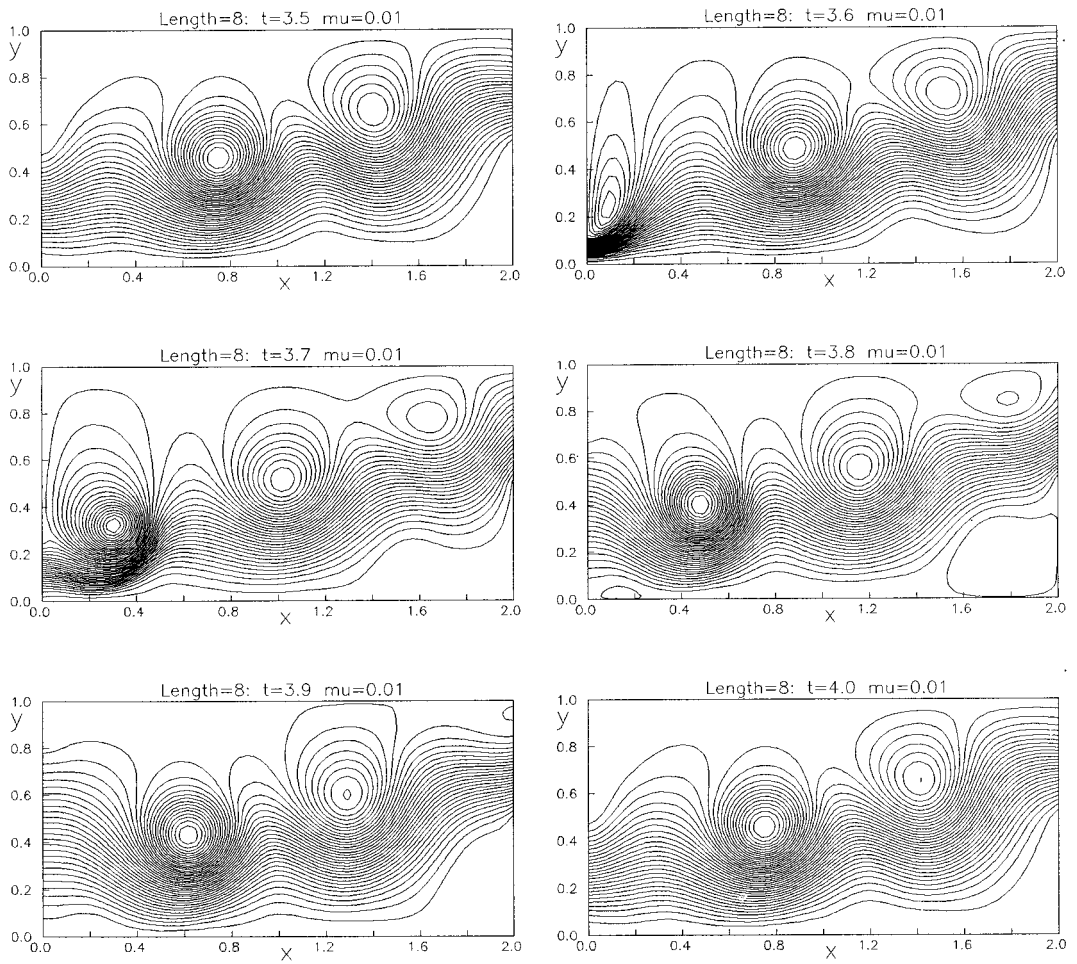

Figure 22. The 'exact' solution; restriction of the real forward-facing step problem.

the literature cited. Some other boundary conditions of the advection type were also tested by us. We briefly comment on them.

Boundary conditions with a drift function simply taken from the previous time step, i.e.,

$$\frac{\partial \mathbf{u}}{\partial t} + u_1 \frac{\partial \mathbf{u}}{\partial n} = \mathbf{0}$$

turns out to be not a good choice on the outflow. They work similar to the 'fixed' conditions.

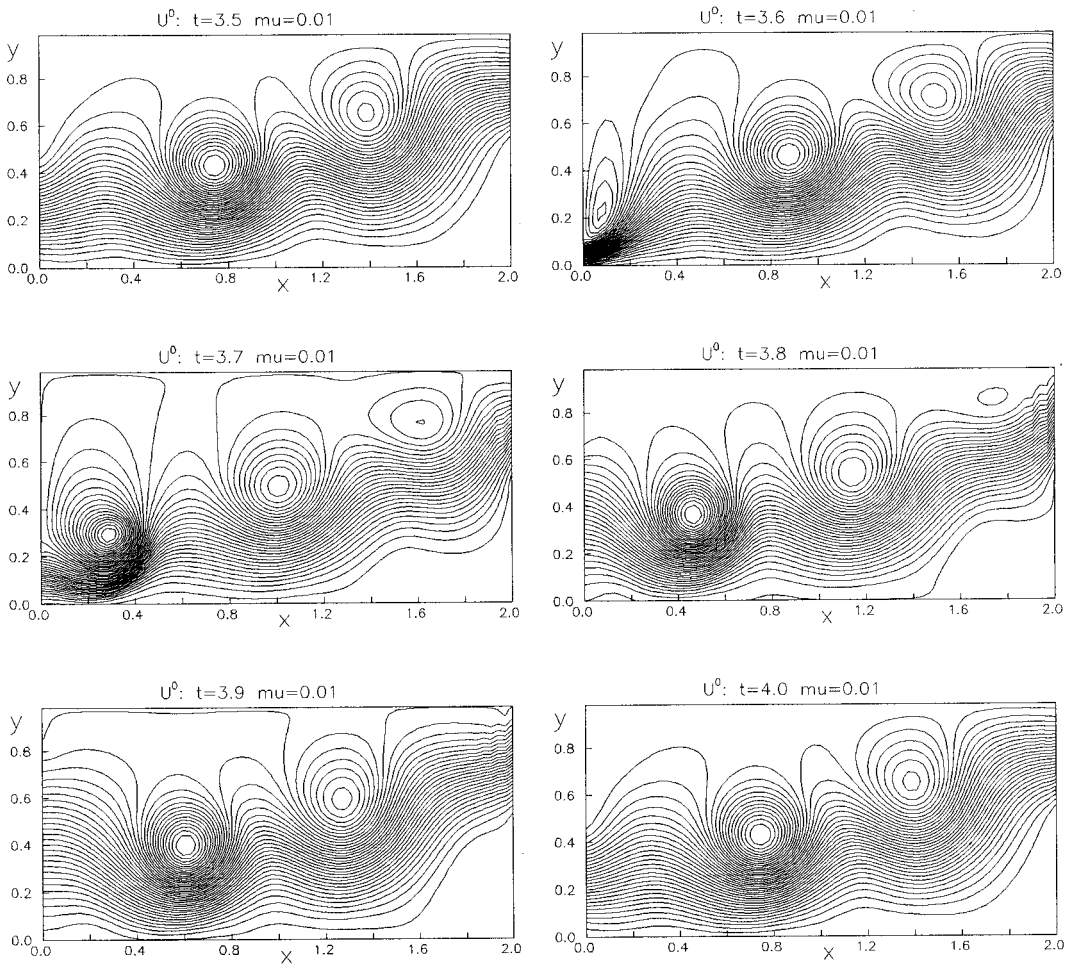

Figure 23. The decay of the main vortex with 'fixed' boundary conditions, [BC] step is on the outlet.

The following boundary conditions:

$$\frac{\partial u_1}{\partial t} + U_1^{(k)} \frac{\partial u_1}{\partial n} = 0, \quad k = 1, 2$$

$$u_2 = 0$$

were also tested and showed themselves to be of the absorbing type. The behavior of the flow was rather like in the case of uniform drift outflow conditions.

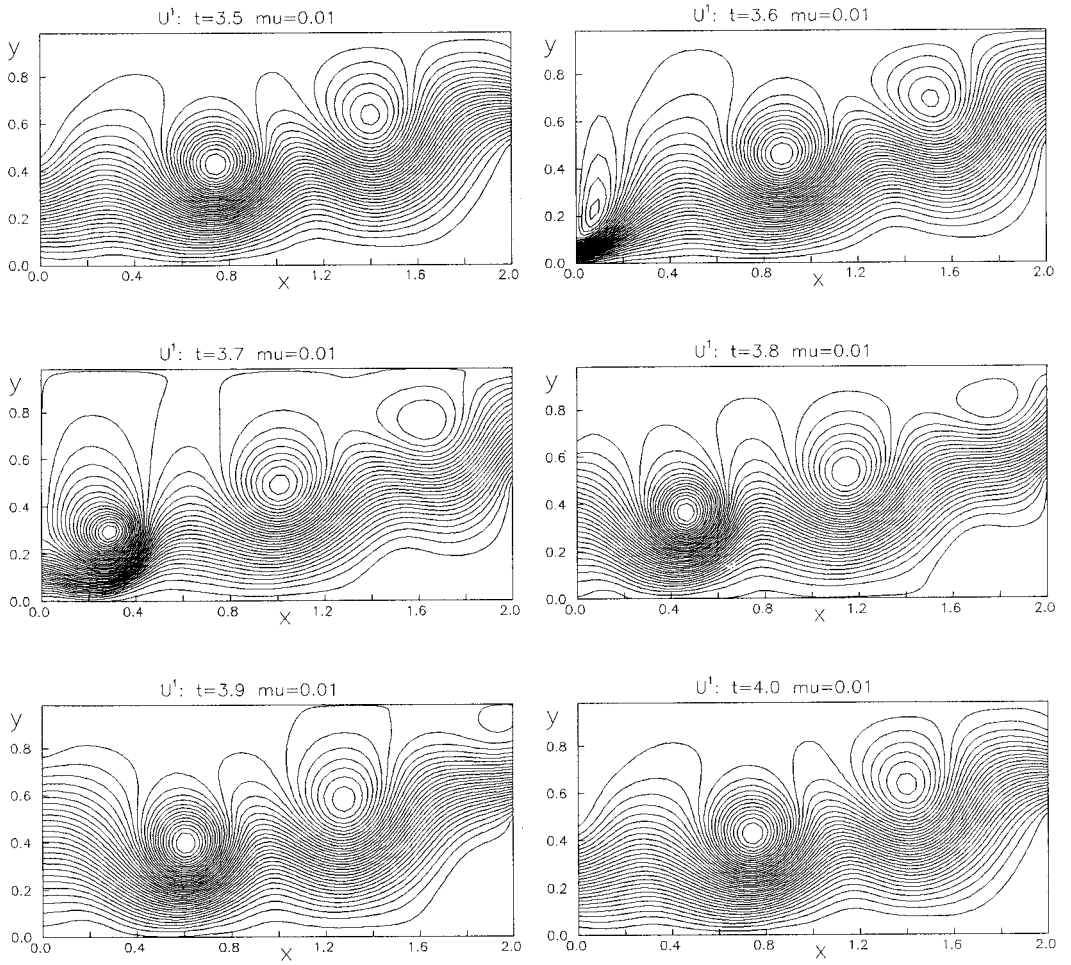

Figure 24. Passing of the main eddy over the boundary with uniform drift conditions, [BC] step is on the outlet.

Resuming the results of all experiments we state that the drift boundary conditions with *appropriate* drift function is the best choice in the considered class of absorbing outflow conditions. They really suppress an upstream influence of the artificial boundary and at the same time they are convenient in computations via various finite methods. When there is no appropriate drift function, the uniform drift conditions seems to be the proper choice. Anyway, the good choice of the drift function in (7) is quite important.

Finally, we propose that a good approximation of u_1, $\partial u_1/\partial n$, and $\partial u_2/\partial n$ on the artificial boundary is of major importance, while the approximation of u_2 is of minor one.

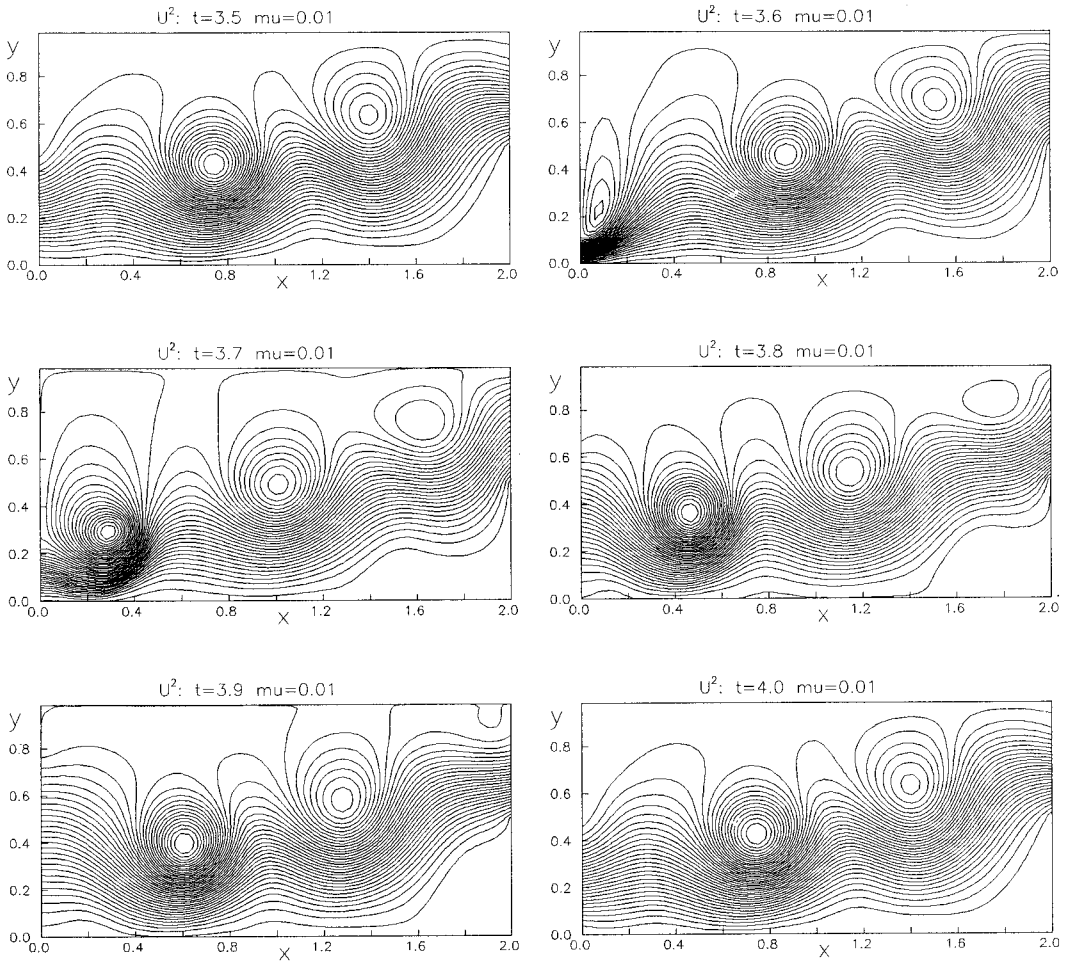

Figure 25. The decay of the main vortex with Poiseuille drift boundary conditions, [BC] step is on the outlet.

Table II. Computing time for RISC-6000 processor (h:min); $\nu = 0.01$, $Re = 10^3$, $t_1 = 5$.

Outlet	τ	$N \times M$	U^0	U^1	U^2
Free	5×10^{-4}	32×64	5:44	5:39	5:39
			5:41	5:40	5:40
[BC] step	2×10^{-4}	64×64	13:23	13:25	13:32

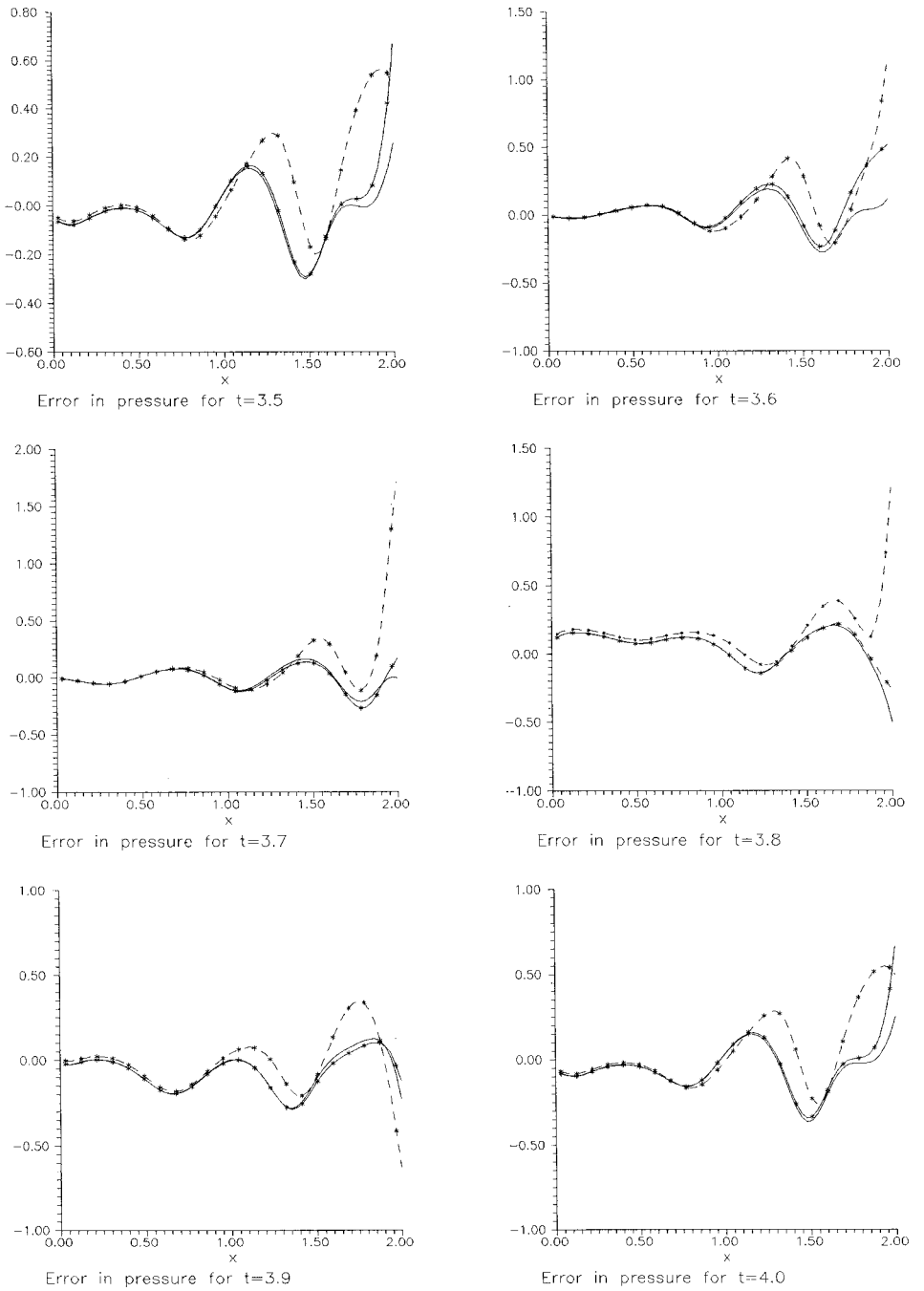

Figure 26. Error in pressure for $y = 0.75$, where $- * -$, b.c. with U^0; $-\times-$, b.c. with U^1; —, b.c. with U^2.

ACKNOWLEDGMENTS

The authors would like to thank E.V. Chizhonkov, G.M. Kobelkov, and A.G. Sokolov for helpful discussions and many useful comments. The work was performed with computer support of the French–Russian A.M. Liapunov Institute of Applied Mathematics and Informatics and was supported in part by RFFI grant 96-01-01254 and by INTAS grant 93-0377-EXT for both authors.

REFERENCES

1. Halpern L, Schatzman M. Artificial boundary conditions for incompressible viscous flows. *SIAM Journal of Mathematics and Analysis* 1989; **20**: 308–353.
2. Hagstrom T. Conditions at the downstream boundary for simulations of viscous, incompressible flow. *SIAM Journal of Science, Statistics and Computers* 1991; **12**: 843–858.
3. Landau LD, Lifshits EM. *Fluid Mechanics*. Pergamon: New York, 1975.
4. Ferm L, Gunstafsson B. A downstream boundary procedure for the Euler equations. *Computers and Fluids* 1982; **10**: 261–276.
5. Johnson C, Nedelec JC. On the coupling of boundary integral and the finite element methods. *Mathematics and Computers* 1980; **35**: 1063–1079.
6. Lenoir M, Tounsi A. The localized finite element method and its application to the 2D seakeeping problem. *SIAM Journal of Numerical Analysis* 1988; **25**: 729–752.
7. Sequeira A. The coupling of boundary integral and finite element methods for the bidimentional steady Stokes problem. *Mathematical Methods and Applications in Science* 1983; **5**: 356–376.
8. Gresho PM. Incompressible fluid dynamics: some fundamental formulation issues. *Annual Reviews in Fluid Mechanics* 1991; **23**: 413–453.
9. Bruneau ChH, Fabrie P. Effective downstream boundary conditions for incompressible Navier–Stokes equations. *International Journal for Numerical Methods in Fluids* 1994; **19**: 693–705.
10. Heywood JG, Rannacher R, Turek S. Artificial boundaries and flux and pressure conditions for the incompressible Navier–Stokes equations. *International Journal for Numerical Methods in Fluids* 1996; **22**: 325–352.
11. Engquist B, Majda A. Absorbing boundary conditions for numerical simulations of waves. *Mathematics and Computers* 1977; **31**: 629–651.
12. Bayliss A, Turkel E. Radiation boundary conditions for wave-like equations. *Communications in Pure and Applied Mathematics* 1980; **33**: 707–725.
13. Clayton R, Engquist B. Absorbing boundary conditions for acoustic and elastic wave equations. *Bulletin of the Seismology Society of America* 1977; **67**: 1529–1540.
14. Engquist B, Majda A. Radiational boundary conditions for acoustic and elastic wave calculations. *Communications in Pure and Applied Mathematics* 1979; **32**: 313–357.
15. Bayliss A, Turkel E. Far field boundary conditions for compressible flow. *Journal of Computational Physics* 1982; **48**: 182–199.
16. Hedstrom GW. Non-reflecting boundary conditions for nonlinear hyperbolic systems. *Journal of Computational Physics* 1979; **30**: 222–237.
17. Rudy DH, Strikwerda JC. A nonreflecting outflow boundary conditions for subsonic Navier–Stokes calculations. *Journal of Computational Physics* 1980; **36**: 55–70.
18. Thompson KW. Time dependent boundary conditions for hyperbolic systems. *Journal of Computational Physics* 1987; **68**: 1–24.
19. Sani RL, Gresho PM. Resume and remarks on the open boundary condition minisymposium. *International Journal for Numerical Methods in Fluids* 1994; **18**: 983–1008.
20. Johansson V. Boundary conditions for open boundaries for the incompressible Navier–Stokes equations. *Journal of Computational Physics* 1993; **105**: 233–251.
21. Jin G, Braza M. A nonreflecting outlet boundary condition for incompressible unsteady Navier–Stokes calculations. *Journal of Computational Physics* 1993; **107**: 239–253.
22. Gustafson K, Halasi K. Vortex dynamics of cavity flows. *Journal of Computational Physics* 1986; **64**: 279–319.
23. Kobelkov GM. On numerical methods of solving the Navier–Stokes equations in 'velocity-pressure' variables. In *Numerical Methods and Applications*, Marchuk C (ed.). CRC Press: New York, 1994; 81–115.
24. Kobelkov GM. Solution of stationary free convection problem. *Doklady Academii Nauk SSSR* 1980; **255**: 277–282.
25. Fletcher CAJ. *Computational Techniques for Fluid Dynamics 2*. Springer: New York, 1988.

26. Ol'shanskii MA. On the numerical solution of the nonstationary Stokes equations. *Russian Journal of Numerical Analysis and Mathematical Modelling* 1995; **10**: 81–92.
27. Temam P. *Navier–Stokes Equations. Theory and Numerical Analysis*. North Holland: Amsterdam, 1979.
28. Nicolaides RA. Analysis and covergence of the MAC scheme I. The linear problem. *SIAM Journal of Numerical Analysis* 1992; **29**: 1579–1591.
29. Armaly BF, Durst F, Pereira JCF, Schonung B. Experimental and theoretical investigation of backward-facing step flow. *Journal of Fluid Mechanics* 1983; **127**: 473–496.

